Title

Polo-like kinase 1 independently controls microtubule-nucleating capacity and size of the centrosome.

Permalink

Journal

Authors

Ohta, Midori
Zhao, Zhiling
Wu, Di
et al.

Publication Date

DOI

Peer reviewed

Polo-like kinase 1 independently controls microtubule-nucleating capacity and size of the centrosome

Midori Ohta[1], Zhiling Zhao[1] , Di Wu[1], Shaohe Wang[1], Jennifer L. Harrison[2] , J. Sebastián Gómez-Cavazos[2], Arshad Desai[1,2,3] , and Karen F. Oegema[1,2,3]

Centrosomes are composed of a centriolar core surrounded by a pericentriolar material (PCM) matrix that docks microtubule-nucleating γ-tubulin complexes. During mitotic entry, the PCM matrix increases in size and nucleating capacity in a process called centrosome maturation. Polo-like kinase 1 (PLK1) is recruited to centrosomes and phosphorylates PCM matrix proteins to drive their self-assembly, which leads to PCM expansion. Here, we show that in addition to controlling PCM expansion, PLK1 independently controls the generation of binding sites for γ-tubulin complexes on the PCM matrix. Selectively preventing the generation of PLK1-dependent γ-tubulin docking sites led to spindle defects and impaired chromosome segregation without affecting PCM expansion, highlighting the importance of phospho-regulated centrosomal γ-tubulin docking sites in spindle assembly. Inhibiting both γ-tubulin docking and PCM expansion by mutating substrate target sites recapitulated the effects of loss of centrosomal PLK1 on the ability of centrosomes to catalyze spindle assembly.

Introduction

During cell division in metazoans, centrosomes catalyze assembly of the mitotic spindle (Basto et al., 2006; Bazzi and Anderson, 2014; Khodjakov and Rieder, 2001; Meitinger et al., 2016; Pintard and Bowerman, 2019; Sir et al., 2013; Wong et al., 2015). Centrosomes are composed of a centriolar core surrounded by a pericentriolar material (PCM) matrix that nucleates and anchors microtubules (Kellogg et al., 1994; Mennella et al., 2014; Woodruff et al., 2014). The PCM matrix forms via the self-assembly of large coiled-coil proteins; the primary structural component of the PCM matrix is CDK5RAP2 in human cells, Centrosomin (Cnn) in *Drosophila melanogaster*, and SPD-5 in *Caenorhabditis elegans* (Woodruff et al., 2014). During mitotic entry, the PCM matrix expands in a process termed centrosome maturation (Palazzo et al., 2000) under the control of Polo-like kinase 1 (PLK1; Cabral et al., 2019; Conduit et al., 2014; Dobbelaere et al., 2008; Haren et al., 2009; Lane and Nigg, 1996; Lee and Rhee, 2011; Woodruff et al., 2015). In *Drosophila* and *C. elegans*, PCM expansion results from the isotropic incorporation of additional PCM matrix molecules (Conduit and Raff, 2015; Laos et al., 2015). In *Drosophila*, PCM matrix expansion has been shown to be driven by a phospho-regulated self-interaction between Cnn molecules in which the Centrosomin motif 2 (CM2)

region at the C-terminus of one Cnn molecule interacts with an internal region in a second Cnn molecule that comprises a leucine zipper with adjacent PLK1 phosphorylation sites that regulate assembly (Citron et al., 2018; Conduit et al., 2014; Feng et al., 2017). In *C. elegans*, a similar set of PLK1 sites has been identified that controls SPD-5 self-assembly (Woodruff et al., 2015).

The PCM matrix docks nucleating complexes containing the tubulin isoform γ-tubulin (Moritz et al., 1995, 1998; Schnackenberg et al., 1998). The large ring-shaped γ-tubulin complexes on the PCM matrix form via the lateral association of smaller Y-shaped hetero-tetrameric complexes that contain two molecules of γ-tubulin supported by a pair of structurally similar γ-tubulin–interacting proteins (e.g., GCP2 and GCP3 in humans; Consolati et al., 2020; Kollman et al., 2011, 2010; Liu et al., 2020; Oegema et al., 1999; Wieczorek et al., 2020b). CDK5RAP2 and Cnn recruit γ-tubulin complexes via a conserved Centrosomin motif 1 (CM1) region in their N-termini (Choi et al., 2010; Fong et al., 2008; Samejima et al., 2008; Zhang and Megraw, 2007). Recent work has shown that a set of helices in the N-terminal domain of some γ-tubulin complex proteins (GCPs) intercalates with 3-α helix microproteins of the Mozart family and that this intercalation can be important for interaction with tethering factors (Huang et al., 2020; Wieczorek

et al., 2020a). For example, the CM1 region of CDK5RAP2 forms a short parallel coiled-coil that interacts with a Mozart (MZT2) intercalated GCP2 subunit in the large γ-tubulin ring complex (Wieczorek et al., 2020a). Consistent with the idea that microtubule nucleating capacity might increase passively as a consequence of expansion of the PCM matrix, interaction of γ-tubulin complexes with the CM1 motif has not been proposed to be directly regulated.

Here, we use the *C. elegans* embryo to test the idea that increased microtubule nucleation by mitotic centrosomes is a passive consequence of PLK1-triggered PCM expansion. Contrary to this idea, we found that PLK1 has two separable functions in centrosome maturation and controls the generation of γ-tubulin complex docking sites independently of PCM expansion. Simultaneously disrupting both processes by mutating critical PLK1 target sites on the PCM matrix recapitulates the effects of loss of PLK1 on the ability of the centrosomes to catalyze spindle assembly. Our results explain how PLK1 remodels the centrosome and indicate that generation of phospho-regulated γ-tubulin docking sites on the PCM matrix is critical for spindle assembly and chromosome segregation.

Results

PCM matrix expansion does not fully account for the function of centrosomal PLK-1

Across metazoans, docking of PLK1 onto CEP192 homologues delivers PLK1 to centrosomes so that it can transform the centrosome during mitotic entry (Alvarez-Rodrigo et al., 2019; Decker et al., 2011; Joukov et al., 2014; Meng et al., 2015). *C. elegans* PLK-1 is recruited to centrosomes by binding of its C-terminal polo boxes to a site, thought to be primed by Cdk1, in the CEP192 homolog SPD-2 (Fig. 1 A; Decker et al., 2011). Centrosomal PLK-1 promotes PCM expansion by phosphorylating a set of residues, including S653 and S658, in the middle region of the PCM matrix component SPD-5 that are required for its self-assembly (Fig. 1 A; Woodruff et al., 2015).

To test the idea that the essential function of centrosomal PLK-1 is to promote PCM matrix expansion, we compared the consequences of preventing the centrosomal targeting of PLK-1 with the consequences of blocking PCM matrix expansion. To disrupt PLK-1 targeting, we expressed WT or PLK-1 docking mutant (PD^mut) SPD-2 from single-copy RNAi-resistant transgenes (Fig. S1 A) in embryos that also expressed in situ–tagged PLK-1::GFP and mCherry::SPD-5 (to enable monitoring of PCM matrix dynamics). Prior work has shown that SPD-2 localizes to centrioles and at a lower level to the surrounding PCM (Kemp et al., 2004; Pelletier et al., 2004); PLK-1 has a similar distribution, although it has been reported to be slightly more focused at centrioles than SPD-2 (Cabral et al., 2019; Magescas et al., 2019; Mittasch et al., 2020). After endogenous SPD-2 depletion, PLK-1::GFP was recruited to centrosomes and kinetochores as expected in embryos expressing transgenic WT SPD-2. By contrast, in embryos expressing PD^mut SPD-2, PLK-1::GFP was recruited to kinetochores, but little to no PLK-1::GFP was detected at centrosomes. The SPD-5 matrix also failed to expand as embryos expressing PD^mut SPD-2 entered mitosis (Fig. 1 B and Video 1). Thus, in agreement with prior work (Decker et al.,

2011), docking of PLK-1 on SPD-2 is required for expansion of the SPD-5 matrix during mitotic entry.

To compare the effects of preventing centrosomal PLK-1 targeting with the consequences of blocking SPD-5 matrix expansion, we generated transgenes encoding GFP fusions with WT SPD-5 or SPD-5 in which two PLK-1 sites essential for expansion (S653 and S658) were mutated to alanine (expansion mutant [Exp^mut] SPD-5; Fig. S1 B and Video 2). Following endogenous SPD-5 depletion, Exp^mut SPD-5 exhibited an expansion defect comparable to that resulting from disrupting centrosomal PLK-1 targeting (Fig. 1 C). However, despite their similar effects on SPD-5 matrix expansion, there was a striking difference in the phenotypes resulting from the two perturbations (Fig. 1 D and Fig. S1 C). Penetrant chromosome segregation defects and embryonic lethality were observed after preventing PLK-1 docking at centrosomes but not after preventing SPD-5 matrix expansion (Fig. 1 D). These results indicate that the centrosomes in SPD-5 Exp^mut embryos, although small, support assembly of a spindle that segregates chromosomes; in addition, they suggest that controlling SPD-5 expansion is not the only function of centrosomal PLK-1 during mitotic entry.

A functional screen identifies putative PLK-1 target sites required to dock γ-tubulin complexes onto the PCM matrix

The results above suggested that there are other sites targeted by centrosomal PLK-1 that are important for spindle assembly and chromosome segregation. To identify such sites, we employed an unbiased strategy (Gómez-Cavazos et al., 2020), mutating putative PLK-1 target sites in SPD-5. In brief, we generated seven strains expressing GFP::SPD-5 from single-copy RNAi-resistant transgenes in which regional clusters of candidate PLK-1 sites were mutated to alanines (Fig. 2 A; and Fig. S1, D and E). The seven cluster mutants, together with GFP-tagged WT and Exp^mut SPD-5, were analyzed following endogenous SPD-5 depletion (Fig. 2 A). WT SPD-5 rescued the embryonic lethality resulting from endogenous SPD-5 depletion, as did Exp^mut SPD-5 and 6 of the alanine cluster mutants. Notably, the Cluster II mutant (Cluster II^mut) was associated with penetrant embryonic lethality. This result suggested that the three putative PLK-1 sites in Cluster II (S170, T178, and T198) provide an essential function.

To assess the function of the putative PLK-1 target sites in Cluster II, we filmed embryos expressing Cluster II^mut GFP::SPD-5. In contrast to Exp^mut SPD-5, Cluster II^mut SPD-5 did not block PCM expansion (Fig. 2, B–D; and Video 2). In fact, Cluster II^mut GFP::SPD-5 continued to accumulate at centrosomes even after levels of WT SPD-5 had plateaued. Despite the increased centrosomal signal, mitotic PCM assembled from Cluster II^mut GFP::SPD-5 remained more compact than PCM assembled from WT GFP::SPD-5; this was particularly evident after anaphase onset (Fig. 2 I and Video 2), when the PCM matrix is subjected to forces that pull on PCM-anchored microtubules and promote PCM dispersal (Enos et al., 2018; Magescas et al., 2019; Mittasch et al., 2020). These results raised the possibility that PCM matrix assembled by Cluster II^mut SPD-5 is defective in the generation of PCM-anchored microtubules.

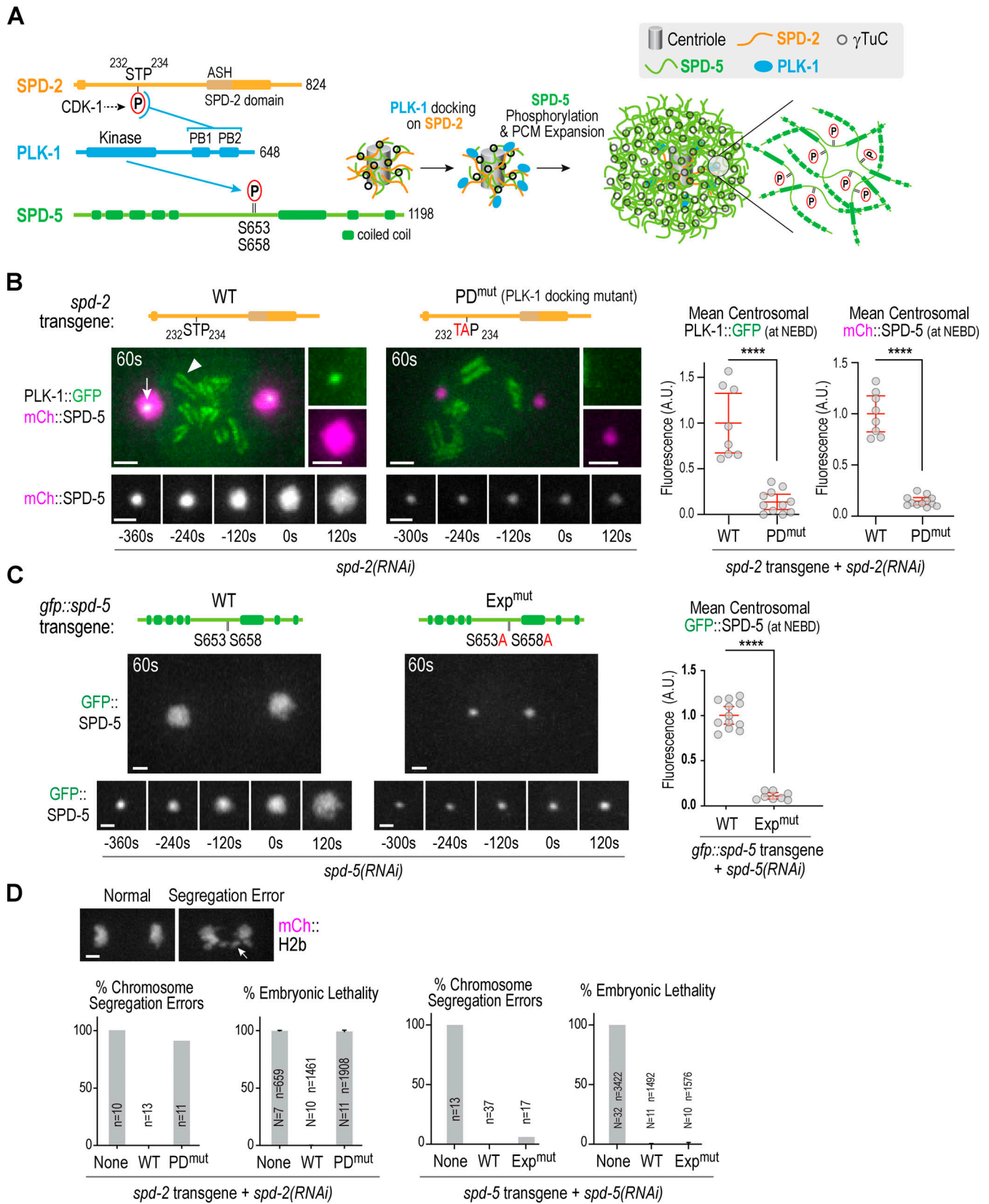The PCM matrix nucleates and anchors microtubules in part due to bound γ-tubulin complexes. Quantitative monitoring of

Figure 1. **Pericentriolar matrix expansion does not fully account for the function of centrosome-localized PLK-1. (A)** Current model for centrosome maturation in *C. elegans*. PLK-1 is recruited to centrosomes by binding of its C-terminal polo boxes (PB1 and PB2) to a site in SPD-2 (CEP192 homologue) thought to be primed by Cdk1 (Thr233). PLK-1 controls PCM expansion by phosphorylating residues, including S653 and S658, in the central region of the PCM matrix component SPD-5 that promote its self-assembly (red circled P indicates phosphorylation). PCM expansion enables docking of a larger number of

γ-tubulin complexes (black rings), thus increasing the capacity of the centrosome to nucleate microtubules. The previously defined ASH (ASPM, SPD-2, Hydin; Ponting, 2006) and SPD-2 (Pelletier et al., 2004) domains in SPD-2 are indicated. **(B and C)** Images of embryos expressing in situ GFP-tagged PLK-1 (green) and in situ mCherry (mCh)-tagged SPD-5 (magenta) in the presence of WT or PD^{mut} SPD-2 after endogenous SPD-2 depletion and WT or expansion-defective (Exp^{mut}) GFP::SPD-5 after endogenous SPD-5 depletion (C). Graphs on right show quantification of centrosomal signals at nuclear envelope breakdown (NEBD). In B, the protein sequence between amino acids 232 and 234 was changed from STP to TAP in PD^{mut} SPD-2 as indicated. Error bars are mean with 95% confidence intervals. P values are from two-tailed t tests. Times in seconds relative to NEBD are shown in top left of large panels and below the smaller panels, which show SPD-5 signal at one centrosome over time. In B, PLK-1 localization to centrosomes (arrow) and kinetochores (arrowhead) in the presence of WT SPD-2 is indicated. **(D)** Chromosome segregation errors and embryonic lethality for the indicated conditions. Top images: example of normal versus defective chromosome segregation, defined as visible chromatin bridges between anaphase chromosome masses in live imaging data. n refers to number of embryos imaged. For embryonic lethality analysis, the mean ± SD is plotted; N refers to number of worms and n to number of embryos scored, respectively. All scale bars, 2 μm.

the centrosomal localization of mCherry-tagged γ-tubulin (TBG-1 in *C. elegans*) revealed that, despite robust SPD-5 matrix expansion, the amount of γ-tubulin recruited to the Cluster II^{mut} SPD-5 matrix was dramatically reduced (Fig. 2, E and F; and Video 3); the ratio of centrosomal γ-tubulin::mCherry to GFP::SPD-5, normalized to be 1 in control embryos expressing WT SPD-5, was close to zero (Fig. 2 H). Exp^{mut} SPD-5 also reduced the amount of centrosomal γ-tubulin (Fig. 2 G and Video 3); however, in this case the ratio of γ-tubulin::mCherry to GFP::SPD-5 at centrosomes was slightly elevated compared with that in embryos expressing WT SPD-5 (Fig. 2 H), indicating that the reduction was a consequence of the decrease in the size of the Exp^{mut} SPD-5 matrix rather than its ability to recruit γ-tubulin complexes. Consistent with normal PCM matrix assembly in Cluster II^{mut} SPD-5 embryos, neither PLK-1 nor SPD-2 centrosomal localization was affected (Fig. S1 F). In Exp^{mut} SPD-5 embryos, SPD-2 and PLK-1 levels were initially normal but then failed to increase following mitotic entry due to the lack of expansion of the SPD-5 matrix (Fig. S1 G). Finally, unlike Exp^{mut} SPD-5, Cluster II^{mut} SPD-5 was associated with significant defects in chromosome segregation (Fig. 2 J), which likely underlie the embryonic lethality observed with Cluster II^{mut} SPD-5 (Fig. 2 A).

Taken together, the above results suggest that PLK-1 independently controls expansion of the PCM matrix and the generation of γ-tubulin docking sites on the PCM matrix by phosphorylation of two different regions of SPD-5.

PLK-1 phosphorylation promotes a direct interaction between SPD-5 and γ-tubulin complexes

Our in vivo work identified a set of putative PLK-1 target sites in the SPD-5 N-terminus (SPD-5^N; S170, T178, and T198) that are essential for γ-tubulin complex recruitment to the PCM matrix. To assess whether PLK-1 phosphorylation at these sites promotes a direct interaction between SPD-5 and γ-tubulin complexes, we established a biochemical reconstitution system. In *C. elegans*, γ-tubulin complexes (here termed Ce γTuCs) are composed of γ-tubulin and two GCPs, GIP-1/GCP3 and GIP-2/GCP2 (Fig. 3 A; Hannak et al., 2001; Sallee et al., 2018). *C. elegans* also has one homologue of the Mozart family of γ-tubulin complex–associated microproteins (MZT-1), which is required to recruit γTuCs to the mitotic PCM (Sallee et al., 2018). This prior work, conducted in intestinal cells, also showed that although the γTuCs at interphase centrioles and the apical noncentrosomal microtubule organizing centers that form in this cell type normally contain MZT-1, MZT-1 is not required for γTuC targeting to these other locations (Sallee et al., 2018); thus,

there are different γTuC targeting modalities, only some of which rely on MZT-1. Using a human cell expression system, we coexpressed the three core γTuC subunits (γ-tubulin, GIP-1, and GIP-2) with and without MZT-1 (Fig. 3 A). In the absence of GIP-2, GIP-1 and γ-tubulin were poorly expressed (Fig. 3 A), indicating that association of the three core complex subunits is important for their stability. However, the three core subunits (γ-tubulin, GIP-1, and GIP-2) could be purified independently of MZT-1 (Fig. 3 A), consistent with the prior in vivo work (Sallee et al., 2018).

In parallel to reconstituting Ce γTuC, we expressed and purified an N-terminal fragment of SPD-5 (aa 1–473, SPD-5^N; Fig. S2 A) designed to lack the SPD-5 region whose phosphorylation controls PCM matrix expansion (Fig. 3 B). SPD-5^N mobility was substantially retarded following incubation with constitutively active PLK-1, with the extent of retardation being slightly reduced by mutation of the Cluster II residues (Fig. 3 B). This result suggested that Cluster II sites are targets of PLK-1 kinase activity in vitro, with additional sites in SPD-5^N also being targeted by PLK-1.

To determine if PLK-1 phosphorylation of Cluster II sites controls interaction of the SPD-5^N with γ-tubulin complexes, we immobilized reconstituted γTuCs on beads, mixed the beads with unphosphorylated or PLK-1–phosphorylated recombinant SPD-5^N, and analyzed bead-bound proteins (Fig. 3 C). PLK-1 phosphorylation substantially enhanced the association of SPD-5^N with γTuC-coated beads. Notably, the ability of PLK-1 to enhance interaction of SPD-5^N with the γTuC was abrogated by mutation of the Cluster II residues (Fig. 3 C). The ability of the γTuC to interact with phosphorylated SPD-5^N also required MZT-1 (Fig. 3 D), consistent with the prior work showing that MZT-1 is required for recruitment of γTuCs to the mitotic PCM in vivo (Sallee et al., 2018). We conclude that MZT-1 is an integral γTuC component required for its PLK-1–dependent docking on the SPD-5 PCM matrix. Consistent with this, Cluster II^{mut} SPD-5 had the same effect on the centrosomal accumulation of in situ–tagged GFP::MZT-1 as it did on γ-tubulin::mCherry (Fig. S2, B and C; and Fig. 2 F). Thus, γ-tubulin complexes with integrated MZT-1 are recruited to SPD-5 in the PCM that is phosphorylated on Cluster II by centrosomal PLK-1.

A single PLK-1 target site is essential for the majority of γ-tubulin complex recruitment to the mitotic PCM matrix

Sequence alignments of SPD-5s from related nematode species indicated that within Cluster II T178 and T198 are conserved, whereas S170 is not (not shown). To evaluate the importance of
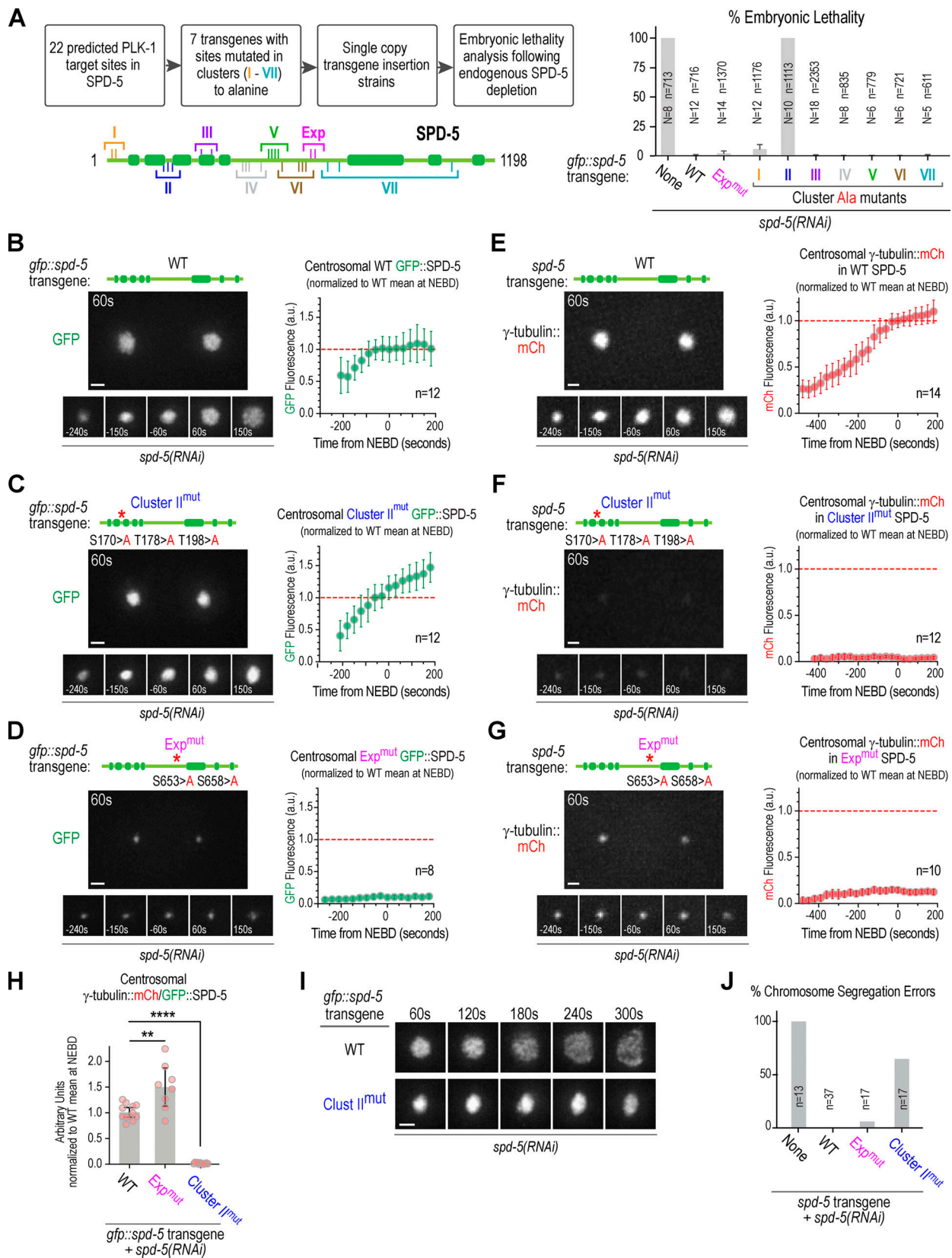
Figure 2. **A putative PLK-1 target site cluster in SPD-5 required to dock γ-tubulin complexes onto the PCM matrix. (A)** Flowchart of screening strategy. Predicted PLK-1 target sites were mutated in seven clusters (schematic), and the consequences on embryonic lethality were assessed. Graph plots embryonic lethality (mean ± SD) for the indicated conditions; *N* refers to number of worms and *n* to number of embryos scored. **(B–G)** Images and quantification of centrosomal intensity of GFP::SPD-5 variants (B–D) or of γ-tubulin::mCherry (E–G) in the presence of the indicated untagged SPD-5 variants (red asterisks

mark the locations of the Cluster II and Expansion blocking mutations); endogenous SPD-5 was depleted in all conditions. Centrosomal fluorescence was plotted after normalizing to the mean at nuclear envelope breakdown (NEBD) for WT GFP::SPD-5 (B–D) or for γ-tubulin::mCherry (mCh) in the presence of WT SPD-5 (E–G); the means for these controls at NEBD are marked with red dashed line in the graphs. Error bars are the 95% confidence intervals. *n* refers to number of centrosomes imaged for each condition. **(H)** Plot of the ratio of centrosomal γ-tubulin::mCherry to GFP::SPD-5 for the indicated mutants. Error bars are the 95% confidence intervals. P values are from two-tailed *t* tests; **, P < 0.01; ****, P < 0.0001. **(I)** Individual centrosomes from the time lapse sequences of embryos expressing WT and Cluster II^{mut} GFP::SPD-5 shown in B and C. Time points highlight the PCM expansion that occurs after anaphase onset when the WT GFP::SPD-5–based matrix disassembles under the influence of cortical pulling forces on matrix-anchored microtubules. **(J)** Chromosome segregation analysis for the indicated conditions. *n* refers to the number of embryos imaged. None, WT, and Exp^{mut} data are reproduced from Fig. 1 D for comparison. Scale bars, 2 μm.

these residues, we analyzed embryonic lethality following their individual mutation. Mutation of S170 had no effect, mutation of T178 resulted in mild (~17%) lethality, and mutation of T198 resulted in penetrant (>95%) lethality (Fig. 3 E). Consistent with this penetrant lethality, sequence analysis of highly divergent nematode species (~400 Mya apart) suggested conservation of a PLK-1 site at the T198 position (Fig. 3 F). A phospho-specific antibody raised against the pT198 site confirmed phosphorylation at this site by PLK-1 in vitro (Fig. 3 F), and mutation of T198 alone significantly compromised the ability of PLK-1 to promote association of SPD-5^N with γTuCs in vitro (Fig. 3 G) and the ability of the SPD-5 matrix to recruit γTuCs in vivo (Fig. 3, H and I; Fig. S2, B and C; and Video 3). These data highlight T198 as being a critical PLK-1 target site whose phosphorylation is required for γ-tubulin complex docking on the mitotic PCM.

We consistently observed slightly more γ-tubulin complex recruitment in embryos expressing T198A relative to Cluster II^{mut} SPD-5 (Fig. 3, H and I; Fig. S2, B and C; and Video 3), suggesting a minor contribution to γ-tubulin complex recruitment by one of the other sites in Cluster II, most likely T178 based on conservation and lethality measurements. In contrast to Cluster II^{mut} SPD-5, which failed to support embryonic viability when untagged or GFP tagged, the residual γ-tubulin complex recruitment supported by T198A SPD-5 was sufficient for embryonic viability when it was untagged but not when it was GFP tagged (Fig. 3 J). Overall, these results suggest that phosphorylation by PLK-1 of SPD-5 T198 plays a major role in γ-tubulin complex docking on the PCM, with phosphorylation on T178 likely playing a minor role. These results also indicate that relatively small amounts of centrosomal γ-tubulin (<20% of normal levels) are sufficient to support embryonic viability.

PLK-1–controlled γ-tubulin complex docking and PCM expansion collaboratively support spindle assembly

The analysis above indicates that PLK-1 has two separable functions during centrosome maturation; it controls γ-tubulin complex docking by phosphorylating a region in the SPD-5 N-terminus and promotes PCM expansion by phosphorylating a region in the middle of SPD-5. To address to what extent these two functions, both working through a common substrate, account for the action of centrosomal PLK-1, we analyzed spindle assembly and chromosome segregation. To define the role of centrosomal PLK-1 in spindle assembly, we analyzed PD^{mut} SPD-2 in a strain with labeled microtubules and chromosomes (Fig. 1 B). Quantitative analysis revealed that disrupting centrosomal PLK-1 recruitment significantly compromised microtubule assembly around centrosomes (assessed by measuring centrosomal

β-tubulin intensity), centrosome separation, and chromosome segregation (Fig. 4, A and C; and Video 4).

When γ-tubulin complex docking or PCM matrix expansion was disrupted individually using the SPD-5 Cluster II or Exp mutants, the phenotypes were significantly milder than disruption of centrosomal PLK-1. In both cases, centrosomal microtubule intensity was reduced to a lesser degree than when centrosomal PLK-1 recruitment was disrupted, and centrosome separation kinetics were not significantly altered (Fig. 4, B and C; and Video 4). To assess if simultaneously disrupting PLK-1–driven γ-tubulin complex docking and PCM expansion recapitulated the effects of preventing PLK-1 centrosomal recruitment, we generated a double Cluster II^{mut} and Exp^{mut} SPD-5. The double-mutant SPD-5 exhibited similar severity defects—in centrosomal microtubule intensity, centrosome separation, and chromosome segregation—as PD^{mut} SPD-2 (Fig. 4, B and C; and Video 4). Thus, the severe spindle assembly defect resulting from disrupting the centrosomal targeting of PLK-1 can be reconstituted by preventing the phosphorylation of two sets of PLK-1 target sites in the substrate SPD-5 that independently control γ-tubulin complex docking and PCM matrix expansion.

Despite essentially identical centrosome separation kinetics, one phenotypic difference between the individual mutant phenotypes was that chromosome segregation defects were significantly higher in the presence of Cluster II^{mut} versus Exp^{mut} SPD-5 (Fig. 4 B; see also Fig. 2 J). We suspect that this difference may arise from the nature of the spindle microtubules in these two conditions. In SPD-5 Exp^{mut} embryos, spindle microtubules are likely generated by SPD-5–anchored γ-tubulin complexes as in control embryos, but there are fewer microtubules because of the lack of PCM expansion. The origin of the microtubules in SPD-5 Cluster II^{mut} embryos, in which the PCM matrix is severely compromised in its ability to dock γ-tubulin complexes, is less clear. One possibility is that the remaining microtubules are generated by γ-tubulin complexes recruited from the cytoplasm that cap microtubule minus ends but are not PCM anchored. As PCM assembly is unaffected in Cluster II^{mut} embryos (Fig. 2 C), a second possibility is that the remaining spindle microtubules are nucleated by γ-tubulin–independent mechanisms involving other PCM-localized factors and/or the ability of centrosomes to locally concentrate soluble tubulin (Baumgart et al., 2019; Woodruff et al., 2017). A serendipitous observation leads us to favor the first possibility. When assessing the effect of Cluster II^{mut} SPD-5 on γ-tubulin complex recruitment, we analyzed the recruitment of in situ GFP-tagged GIP-2, which, like γ-tubulin::mCherry and GFP::MZT-1, failed to localize to the mitotic PCM in Cluster II^{mut} SPD-5 embryos (Fig. S3 A). However, there was a
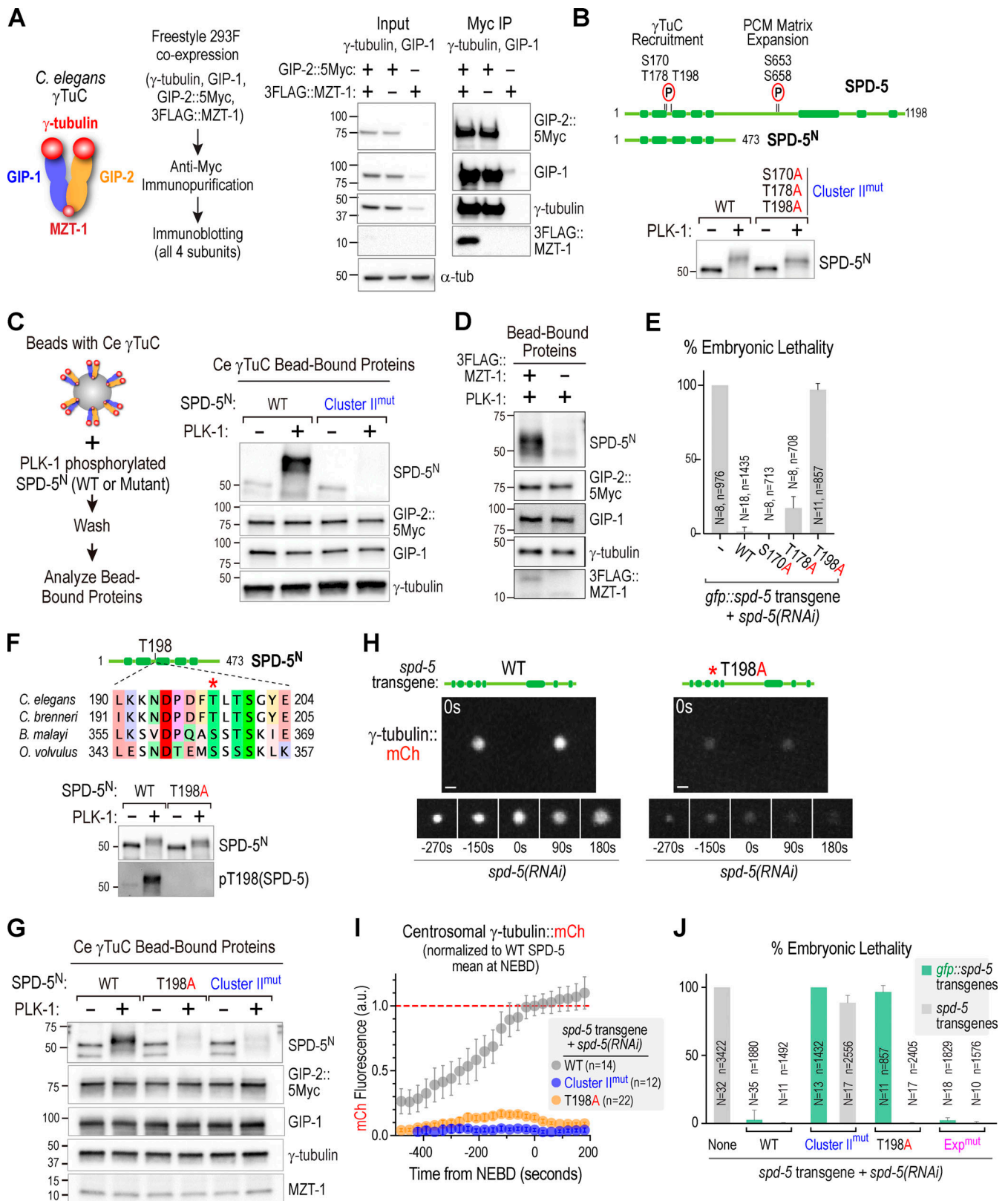
Figure 3. **PLK-1 phosphorylation controls a direct interaction between SPD-5 and the γ-tubulin complex. (A)** Reconstitution of the *C. elegans* γ-tubulin complex (schematic) by coexpression in mammalian cells (flowchart in middle). Plasmids encoding γ-tubulin, GIP-1, GIP-2, and MZT-1 were cotransfected, and the Myc tag on GIP-2 was used to immunoprecipitate the complex (Myc IP). Immunoblots show input (left blot, α-tubulin [α-tub] was used as a loading control) and anti-Myc immunoprecipitated material (right blot) for the indicated conditions. **(B)** Schematic showing the locations in SPD-5 of the clusters of PLK-1 phosphorylation sites (indicated by red circled P) implicated in γ-tubulin recruitment (Cluster II; S170, T178, and T198) and PCM matrix expansion (S653 and S658). A SPD-5[N] fragment that lacks the PCM expansion sites was bacterially expressed and purified. Blot shows effect of incubation of SPD-5[N] variants with or

without PLK-1 in the presence of ATP for 1 h at 23°C. **(C)** Left: Schematic of analysis of interaction of γ-tubulin complexes immobilized on beads, with SPD-5^N (either WT or Cluster II^{mut}) preincubated with or without PLK-1. Right: Blots of bead-bound components after incubation and isolation are shown; FLAG-tagged MZT-1 was present but was not blotted here. **(D)** Analysis of interaction of PLK-1–phosphorylated SPD-5^N with γ-tubulin complexes reconstituted with or without FLAG-tagged MZT-1. **(E)** Graph of embryonic lethality (mean ± SD); N refers to number of worms and n to number of embryos. **(F)** Top: Alignment of sequences from divergent nematodes highlighting potential conservation of the critical T198 site. Bottom: Indicated SPD-5^N variants incubated with or without PLK-1 and immunoblotted to detect total SPD-5 (top) and phosphorylation of T198 (bottom), using a phospho-specific antibody (pT198). **(G)** Analysis of γ-tubulin complex binding, conducted as in C, for the indicated conditions. **(H and I)** Representative images and quantification of γ-tubulin:: mCherry (mCh) recruitment to centrosomes for the indicated conditions. The red asterisk marks the location of the T198A mutation in SPD-5. Dashed line marks the amount of γ-tubulin at centrosomes at nuclear envelope breakdown (NEBD) in embryos expressing WT SPD-5. Error bars are the 95% confidence interval. Times are in seconds after NEBD. Scale bar, 2 µm. Data for WT and Cluster II^{mut} SPD-5 is reproduced from Fig. 2, E and F for comparison. **(J)** Embryonic lethality is plotted for the indicated conditions. Data for the non–gfp-containing transgene (None, WT, and Exp^{mut}) conditions is the same as that shown in Fig. 1 D and is reproduced here for comparison. N refers to the number of worms and n to the number of embryos scored. Error bars are the standard deviation. *B. malayi*, *Brugia malayi*; *C. brenneri*, *Caenorhabditis brenneri*; *O. volvulus*, *Onchocerca volvulus*.

Discussion

Here, we address the mechanism by which PLK1 transforms the centrosome during mitotic entry to support spindle assembly. Our results suggest that PCM expansion is not sufficient to account for the function of centrosomal PLK1. Instead, centrosome maturation during mitotic entry is accomplished via the action of two separable PLK1-dependent processes, PCM matrix expansion and γ-tubulin complex docking, which collaborate to increase the nucleating capacity of centrosomes for spindle assembly (Fig. 4 D).

PCM matrix components: Conserved modes of regulation?

C. elegans SPD-5 shares many properties with the PCM matrix components Cnn and CDK5RAP2. Expansion of the Cnn-based PCM matrix in *Drosophila* occurs through PLK1 phospho-regulated self-assembly (Citron et al., 2018; Conduit et al., 2014; Feng et al., 2017). Sequence analysis indicated that nematode SPD-5s have regions with homology to the domains of Cnn that are critical for this PLK1-regulated self-assembly (Fig. S3, C and D). A hallmark feature of *Drosophila* Cnn and human CDK5RAP2 is the presence of a conserved CM1 motif, which directly interacts with γ-tubulin complexes (Choi et al., 2010; Fong et al., 2008; Samejima et al., 2008; Zhang and Megraw, 2007). Structural work has shown that the CM1 region of human CDK5RAP2 forms a short parallel coiled-coil that interacts with a MZT2-intercalated GCP2 subunit in the γ-tubulin complex (Wieczorek et al., 2020a). The CM1 motif interaction with γ-tubulin complexes has not been found to require phosphorylation. Sequence analysis suggests the presence of a divergent CM1-like domain in nematode SPD-5s, ~70 aa N-terminal to the critical PLK-1 target sites identified here (Fig. 4 E). Based on structural work with human proteins and given that the interaction we characterize between PLK-1 phosphorylated SPD-5

and γ-tubulin complexes depends on *C. elegans* Mozart (MZT-1), we speculate that PLK-1 phosphorylation generates γ-tubulin docking sites by unmasking a CM1-like domain on SPD-5 molecules that are incorporated into the PCM matrix (Fig. 4 F). In this model, PLK-1 phosphorylation would release autoinhibition intrinsic to the SPD-5^N to expose the CM1-like γ-tubulin docking site on SPD-5. An appealing feature of this model is that it would constrain association with γ-tubulin complexes to SPD-5 assembled into the PCM matrix, in the vicinity of concentrated PLK-1 activity.

We note that in human cells phosphorylation by LRRK1 of Ser140 of CDK5RAP2, 54 aa distal to the CM1 domain, has been proposed to regulate interaction with γ-tubulin complexes (Hanafusa et al., 2015). The identified LRRK1 target site (S140) is not conserved even in vertebrates; however, there are PLK1 sites in the region following the core CM1 motif in vertebrate CDK5RAP2 and *Drosophila* Cnn that may act in a manner similar to the sites we describe here for SPD-5. Future experimental analysis in different organisms, together with continuing analysis of SPD-5 in *C. elegans* based on the sequence comparisons shown here, will be important to test these ideas.

Overall, the results presented here explain how centrosome-targeted PLK-1 remodels the centrosome for spindle assembly and reveal tight phospho-regulation of γ-tubulin docking on the PCM matrix during the transition from interphase to mitosis. We suggest that similar phosphoregulation may be employed in different contexts by diverse γ-tubulin complex tethering factors to ensure the spatial regulation of microtubule nucleation.

Materials and methods

C. elegans strains

C. elegans strains (listed in Table S1) were maintained at 16°C. Single-copy transgenes were generated by using the transposon-based MosSCI method (Frøkjær-Jensen et al., 2008) to recombine them into specific chromosomal sites. Transgenes were cloned into pCFJ151 and injected into strains with specific Mos transposon insertions to recombine them into the ttTi5605 site on Chromosome (Chr) II or the Uni V oxTi365 site on Chr V. Transgenes were generated by injecting a mixture of the pCFJ151-derived repairing plasmid containing the Cb-unc-119 selection marker and appropriate homology arms (50–100 ng/ µl), transposase plasmid (pCFJ601 encoding the Mos1 transposase under the Peft-3 promoter, 50 ng/µl), and four plasmids
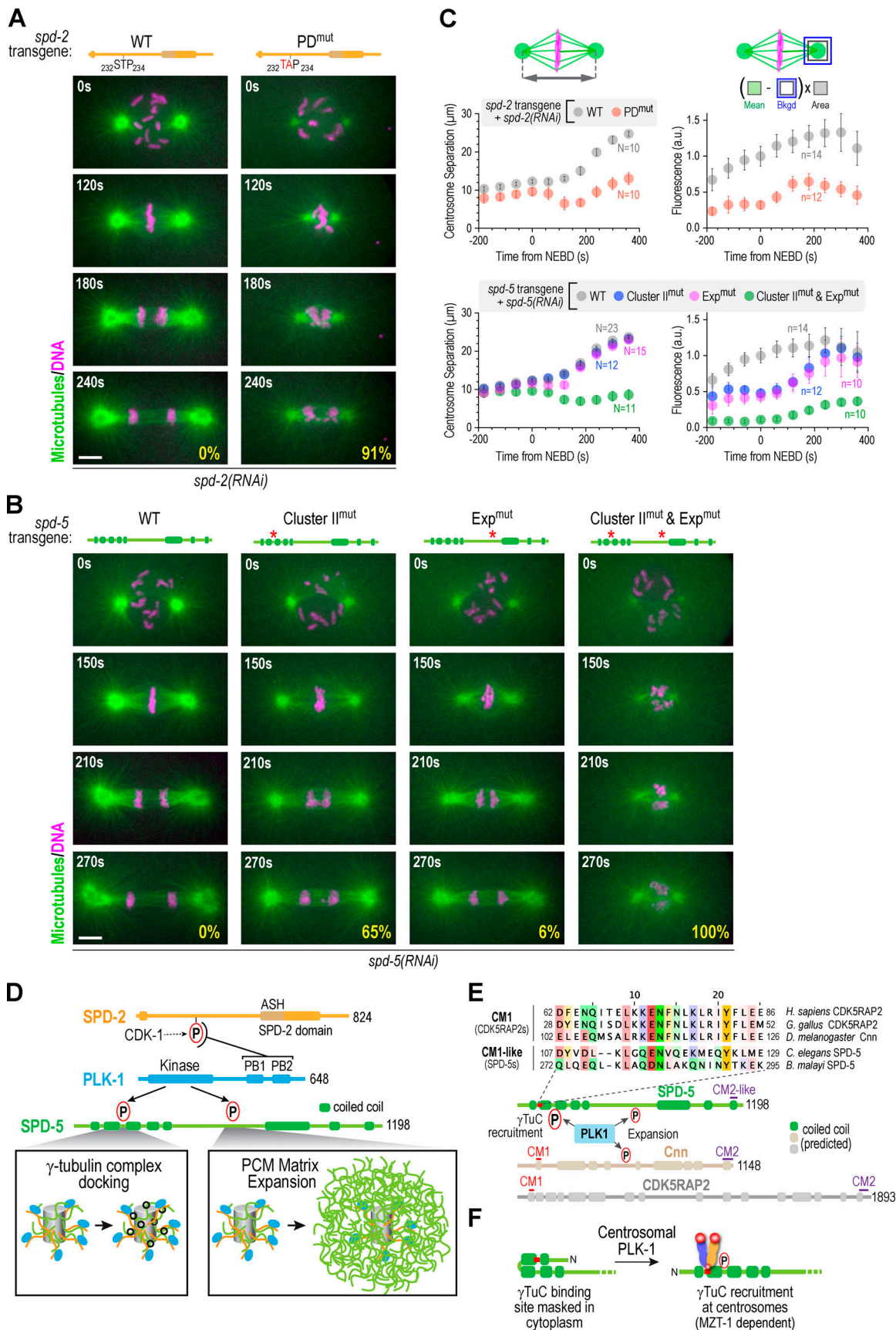
Figure 4. **Inhibiting γ-tubulin docking and PCM expansion by mutating substrate target sites recapitulate the effects of loss of centrosomal PLK-1 on the ability of centrosomes to catalyze spindle assembly. (A and B)** Images of GFP::β-tubulin (green) and mCherry::histone (magenta) in embryos expressing

the indicated untagged SPD-2 (A) or SPD-5 (B) variants with endogenous SPD-2 (A) or SPD-5 (B) depleted. The protein sequence between amino acids 232 and 234 was changed from STP to TAP in PD^mut SPD-2 as indicated. Red asterisks mark the mutated phosphorylation site clusters in SPD-5. Times in the top left of each panel are seconds after NEBD. Percentages of chromosome segregation errors are in yellow at the bottom right of the last panel of each sequence. Chromosome segregation data for conditions other than the double mutant are the same as that shown in Fig. 1 D and Fig. 2 J and are shown here for comparison. Scale bars are 5 µm. **(C)** Quantification of centrosome separation (left) or centrosomal β-tubulin intensity (right) for the indicated conditions. Error bars are the 95% confidence intervals. *N* refers to number of embryos and *n* to number of centrosomes scored. **(D)** Schematic depicting independent phospho-regulation by centrosome-localized PLK-1 of γ-tubulin recruitment and PCM expansion through phosphorylation of PLK-1 site clusters (red circled P) in distinct SPD-5 regions. Black circles and other symbols in the schematics are defined as in Fig. 1 A. **(E)** Sequence alignments supporting nematode SPD-5s being divergent orthologues of CDK5RAP2 and Cnn. SPD-5s from distantly related nematodes (∼400 Mya apart) have a CM1-like motif N-terminal to the key phospho-regulated sites identified here (see Fig. 3 F). SPD-5 also has a CM2-like motif at its C-terminus (Fig. S3 C) and a central PReM-like region (Fig. S3 D). **(F)** Speculative model for mechanism of phospho-regulated γ-tubulin complex recruitment. The CM1-like recruitment site is masked in unphosphorylated cytoplasmic SPD-5. Phosphorylation at centrosomes unmasks the binding site, leading to γ-tubulin complex recruitment specifically on PCM matrix-assembled SPD-5. *B. malayi*, *Brugia malayi*; *G. gallus*, *Gallus gallus*; *H. sapiens*, *Homo sapiens*; PReM, phospho-regulated multimerization. NEBD, nuclear envelope breakdown; Bkgd, background; ASH; ASPM; SPD-2, Hydin domain.

encoding markers for negative selection against chromosomal arrays (pMA122 [Phsp-16.41::peel-1, 10 ng/µl], pCFJ90 [Pmyo-2::mCherry, 2.5 ng/µl], pCFJ104 [Pmyo-3::mCherry, 5 ng/µl], and pGH8 [Prab-3::mCherry, 10 ng/µl]) into strains EG6429 (ttTi5605, Chr II) or EG8082 (oxTi365, Chr V). After 1 wk, the progeny of injected worms were heat-shocked at 34°C for 3 h to induce the expression of PEEL-1 to kill worms containing extra chromosomal arrays. Moving worms without fluorescent markers were identified as candidates, and PCR across the junctions on both sides of the integration site was used to confirm transgene integration in their progeny.

Generation of single-copy insertion transgenes

We had previously generated RNAi-resistant transgenes encoding SPD-2 (Shimanovskaya et al., 2014) and SPD-5 (Woodruff et al., 2015). The same replacement strategies (Fig. S1, A and B) were used to generate the SPD-2 and SPD-5 encoding transgenes described here. Transgenes were generated by PCR amplification of their respective genomic loci. The *spd-2* transgene included a 3,043-bp region upstream of the start codon and 546 bp downstream of the stop codon. As the high level of repetitive sequence in the endogenous *spd-5* promoter made the single-copy insertion procedure inefficient, the *spd-5* transgenes were driven by the *spd-2* promoter and included 577 bp downstream of the stop codon. Segments of the *spd-2* and *spd-5* transgenes were modified as indicated (Fig. S1, A and B) to make the transgenes RNAi resistant without altering coding information. To generate the strains expressing transgenic GFP::SPD-5 with the individual S170A, T178A, and T198A mutations (used in Fig. 3, E and J), CRISPR was used as previously described (Hattersley et al., 2018) to directly introduce the mutations into the reencoded region of the WT *spd-5* transgene. Worms from the strain OD2435 were injected with purified Cas9 mixed with crRNA and trans-activating crispr RNA (tracrRNA; Integrated DNA Technologies) and an appropriate repair template (S170A mutation: crRNA 5′-GGAGTTAGAACTCTCAGCTA-3′, repair template 5′-TCAAATGAAGGAGTTCGAAGCTCAGAAGCACGCTATGGAAGA GCGCATTAAGGAGTTAGAGCTCGCTGCTACTGACGCTAATAA TACGACCGTTGGATCATTTCGAGGAACACTCGATGATATCCT CAAGAAG-3′; T178A mutation: crRNA 5′-GACGCTAATAATACG ACCGT-3′, repair template 5′-GAAGCACGCTATGGAAGAGCG CATTAAGGAGTTAGAACTCTCAGCTACGGACGCTAATAACAC TGCAGTTGGATCATTTCGAGGAACACTCGATGATATCCTCAA

GAAGAATGACCCAGACTTTACT-3′; and T198A mutation: crRNA 5′-CTGAAGTAAGAGTAAAGTCT-3′, repair template 5′-CGGAAC TCGAAGACCACATCCAACAGCTTAGACAGGAGCTCGACGACC AAGCAGCACGACTTGCAGATTCTGAAAACGTTAGAGCACAGCTGG AAGCTGCTACTGGGCAGGGTATTCTGGGA-3′). Strains with the correct edit were identified by PCR with the following primer sets (S170A and T178A: 5′-GAAGCGTCGCAGAAGAGAGT-3′ and 5′-CTTCCAGCTGTGCTCTAACG-3′ and T198A: 5′-TGTTCAAGA GAAAATGGAGCAA-3′ and 5′-GTTTGGGACCATTGCGTTAC-3′) followed by digestion with a diagnostic restriction site introduced during the edit (S170A: SacI; T178A: PstI; and T198A: Bsu36I) and then confirmed by sequencing.

RNAi

Single-stranded RNAs were synthesized in 50 µl T3 and T7 reactions (MEGAscript; Invitrogen) using gel-purified DNA templates generated by PCR from N2 genomic DNA using oligonucleotides containing T3 or T7 promoters (Table S2). Reactions were cleaned using the MEGAclear kit (Invitrogen), and the 50-µl T3 and T7 reactions were mixed with 50 µl of 3× soaking buffer (32.7 mM Na_2HPO4, 16.5 mM KH_2PO_4, 6.3 mM NaCl, and 14.1 mM NH_4Cl) and annealed (68°C for 10 min followed by 37°C for 30 min). For the depletions, double-stranded RNAs (dsRNAs) were injected at a concentration of at least 1.3 µg/µl. L4 hermaphrodites were injected with dsRNA and incubated at 16°C. To assess embryonic lethality after RNAi-mediated depletion, L4 hermaphrodites were injected with dsRNA and incubated at 16°C for 48 h. Worms were singled and allowed to lay embryos at 16°C for 24 h. Adult worms were removed, and all embryos and hatchlings were counted after an additional 24 h (Fig. S1 C). For live imaging of early embryos after RNAi, L4 hermaphrodites were injected with dsRNAs and incubated at 16°C for 48 h before dissection to isolated embryos for imaging.

Antibodies

Rabbit antibodies against SPD-5 (392–550 aa; used at 1 µg/ml for immunoblotting; Dammermann et al., 2004) and γ-tubulin (428–444 aa; used at 1 µg/ml for immunoblotting; Hannak et al., 2001) were previously described. Antibodies against GIP-1 (used 1 µg/ml for immunoblotting) were generated by injecting a GST fusion with GIP aa 1–150 into a rabbit and affinity purifying the antibodies from serum using standard procedures (Harlow and Lane, 1988). A rabbit polyclonal antibody against phosphorylated

T198 in SPD-5 was raised against a phosphorylated peptide KNDPDF-[pT]-LTSGYEE, where [pT] is a phosphorylated threonine residue (Pacific Immunology). The following antibodies were purchased from commercial sources, with their working concentrations indicated in parentheses: mouse anti-α-tubulin (1:5,000 for immunoblotting; DM1A; Sigma-Aldrich); anti-FLAG (1:1,000 for immunoblotting; F1804; Sigma-Aldrich); and anti-Myc (1:5,000 for immunoblotting; monoclonal 9E10; M4439; Sigma-Aldrich). Secondary antibodies were purchased from Jackson ImmunoResearch and GE Healthcare.

Live imaging

Embryos for live-imaging experiments were obtained by dissecting gravid adult hermaphrodites in M9 buffer (42 mM Na_2HPO4, 22 mM KH_2PO_4, 86 mM NaCl, and 1 mM $MgSO_4$). One-cell embryos were transferred with a mouth pipette onto a 2% agarose pad, overlaid with a 22 × 22-mm coverslip, and imaged using a spinning disk confocal system (Andor Revolution XD Confocal System; Andor Technology) with a confocal scanner unit (CSU-10; Yokogawa) mounted on an inverted microscope (TE2000-E; Nikon) equipped with a 60× 1.4 Plan-Apochromat objective or a 100× 1.4 Plan-Apochromat objective, solid-state 100-mW lasers, and an electron multiplication back-thinned charge-coupled device camera (iXon; Andor Technology) or an inverted microscope (Axio Observer.Z1; Carl Zeiss) equipped with a spinning-disk confocal head (CSU-X1; Yokogawa) and a 63× 1.4 NA Plan Apochromat lens (Zeiss) or a 100× 1.3 EC Plan Neofluar lens (Zeiss) in a temperature-controlled room at 20°C. Images of centrosomal fluorescence and chromosome segregation were acquired every 30 or 60 s by collecting 9–12 z-planes at 1.0-μm intervals or 11 z-planes at 1.5-μm intervals without binning. Imaging was initiated in one-cell embryos between centrosome separation and pronuclear meeting and was terminated after initiation of cytokinesis.

Image analysis

All images were processed and analyzed using ImageJ (National Institutes of Health). For figure construction, final image panels were scaled for presentation in Photoshop (Adobe Creative Cloud). A gamma of 1.5 was applied for images of mCherry and GFP-tagged SPD-5, and a gamma of 1.2 was applied to images of γ-tubulin::mCherry, GFP::MZT-1, GIP-2::GFP, and GFP::β-tubulin to allow visualization of centrosomes in the mutants, while not oversaturating the signal in the WT centrosomes. Centrosomal fluorescence in Fig. 1, B and C; Fig. 2, B–H; Fig. 3 I; Fig. S1 F; Fig. S2 C; and Fig. S3 A was quantified from maximum-intensity projections of entire z-stacks. Centrosomal PLK-1::GFP fluorescence (Fig. 1 B, Fig. S1 F, and Fig. S1 G) and microtubule intensity (Fig. 4 C) were quantified from maximum-intensity projections of the portion of the z-stack containing the centrosomes. To quantify centrosomal fluorescence, a fixed-size box was drawn around the centrosome at each time point (smallest box that could enclose the centrosomal signal at the largest point in the image sequence; box size varied depending on marker and imaging conditions), along with a box 1 pixel larger on each side in both dimensions. The per-pixel background was calculated as [(integrated intensity in the larger box – integrated intensity in the smaller box)/(area of larger box – area of smaller box)]. The centrosomal signal was: (integrated intensity in the smaller box) – (area of the smaller box) * (per-pixel background).

Protein expression and purification

GST-tagged SPD-5[N] proteins were expressed in BL21(DE3)pLysS *Escherichia coli* from DNA constructs cloned into a pGEX-6P-1 vector. When the bacterial cultures reached an OD600 of 0.6, protein expression was induced for 16–18 h at 15°C by addition of IPTG to 0.3 mM. Cells were washed once with cold PBS and flash frozen in liquid nitrogen. Pelleted cells were resuspended in PBS with 250 mM NaCl, 10 mM EGTA, 10 mM EDTA, 0.1% Tween, 200 μg/ml lysozyme, 2 mM benzamidine, and EDTA-free protease inhibitor cocktail (Roche) and were lysed by sonication. After 20-min centrifugation at 40,000 rpm in a 45 Ti rotor (Beckman) at 4°C, cleared cell lysates were incubated with glutathione agarose (Sigma-Aldrich) for 2 h at 4°C. The resin was then washed 2× 30 ml with washing buffer (PBS containing 250 mM NaCl, 1 mM β-mercaptoethanol, and 2 mM benzamidine) followed by incubation with 10 ml washing buffer containing 5 mM ATP for 10 min at 4°C to reduce nonspecific interactions with heatshock proteins. After the incubation, the resin was further washed three times with washing buffer and incubated with PreScission protease (Eton Bioscience) in elution buffer (20 mM Tris-Cl, pH 8.0, 150 mM NaCl, and 1 mM DTT) overnight at 4°C to elute the SPD-5[N] protein by cleavage from the GST tag. The supernatant was collected the next day and stored at 4°C. PLK-1 T194D, purified from Sf9 cells, was a gift from Jeffrey Woodruff (UT Southwestern Medical Center, Dallas, TX).

Purification of reconstituted *C. elegans* γ-tubulin complexes

The *C. elegans* γ-tubulin complex was reconstituted by coexpression in human FreeStyle 293-F cells (Thermo Fisher Scientific). The GIP-2 and γ-tubulin (TBG-1) coding sequences were amplified by PCR from an N2 cDNA library. For MZT-1 and GIP-1, coding sequences optimized for human cell expression were synthesized (GENEWIZ). Sequences encoding Myc-tagged GIP-2, FLAG-tagged MZT-1, GIP-1, or *C. elegans* γ-tubulin were cloned into human expression vectors driven by the CMV promoter (Table S3) and cotransfected into FreeStyle 293-F cells (Thermo Fisher Scientific). The empty 5Myc plasmid (CS2P, #17095; Addgene) or 3FLAG plasmid (p3XFLAG-CMV-7.1, #E7533; Sigma-Aldrich) were used as negative controls. Cell transfection was performed using FreeStyle MAX Reagent and OptiPRO SFM serum-free medium according to the manufacturer's guidelines (Thermo Fisher Scientific). 10 ml of cells at 10^6 cells/ml was transfected with a total of 12.5 μg DNA constructs. 43–48 h after transfection, cells were harvested and washed with PBS. The cells were resuspended in lysis buffer (20 mM Tris/HCl, pH 7.5, 50 mM NaCl, 1% Triton X-100, 5 mM EGTA, 1 mM DTT, 2 mM $MgCl_2$, and EDTA-free protease inhibitor cocktail; Roche) and lysed in an ice-cold sonicating water bath for 5 min. After 15-min centrifugation at 15,000× *g* at 4°C, the whole-cell lysates were incubated with Pierce Anti–c-Myc magnetic beads (Thermo Fisher Scientific) for 2 h at 4°C. The beads were washed five times with lysis buffer and used for pull-down assay or resuspended in SDS sample buffer. For immunoblotting, equal volumes of samples were run on Mini-PROTEAN gels (Bio-Rad) and

transferred to polyvinylidene difluoride membranes using a Trans-Blot Turbo system (Bio-Rad). Blocking and antibody incubations were performed in TBS-T plus 5% nonfat dry milk or in TBS-T plus 5% BSA. Immunoblotting was performed as described above.

Kinase and pulldown assays

For the pulldown assays in Fig. 3, 1.5 µM SPD-5[N] proteins was mixed with 200 nM constitutively active PLK-1 T194D (gift from Jeffrey Woodruff) in kinase buffer (20 mM Tris-Cl, pH 7.5, 50 mM NaCl, 10 mM MgCl2, 0.2 mM ATP, and 1 mM DTT). After incubation for 1 h at 23°C, proteins were mixed with Myc beads–bound γ-tubulin complexes in lysis buffer and incubated for 2 h at 4°C. The final concentration of SPD-5[N] was 75 nM. The beads were washed five times with lysis buffer and resuspended in sample buffer before analysis on SDS-PAGE.

Screen for PLK-1 putative phosphorylation sites

Potential PLK-1 phosphorylation sites in SPD-5 were identified using the kinase-specific phosphorylation site prediction system (Xue et al., 2005). Protein sequences in FASTA format were entered, and threshold setting was set to ALL. A list of candidate PLK-1 sites for each target protein was generated using the algorithm shown in Fig. S1 D, and the selected sites were mutated in regional clusters.

Statistical analysis

Statistical analysis was conducted using Prism v8 (GraphPad). P values were determined using unpaired two-tailed t tests assuming equal SD. $P > 0.05$ (NS), $P < 0.05$ (*), $P < 0.01$ (**), $P < 0.001$ (***), and $P < 0.0001$ (****). Data distribution was assumed to be normal, but this was not formally tested.

Online supplemental material

Fig. S1 presents the transgene replacement systems for SPD-2 and SPD-5, the method for identifying putative PLK-1 sites in SPD-5, and analysis of PLK-1 and SPD-2 centrosomal localization in Cluster II[mut] and Exp[mut] SPD-5. Fig. S2 (related to Fig. 3) analyzes GFP::MZT-1 localization. Fig. S3 (related to Fig. 4) shows that in situ–tagged GIP-2::GFP exhibits a synthetic spindle assembly phenotype when combined with Cluster II[mut] SPD-5. Video 1 shows that centrosomal PLK-1 is required for PCM expansion during mitotic entry. Video 2 shows that the putative PLK-1 target site Cluster II[mut] SPD-5 did not block PCM expansion. Video 3 shows that the PLK-1 target site Cluster II in SPD-5 is required to dock γ-tubulin complexes onto the PCM matrix. Video 4 shows that PLK-1–controlled γ-tubulin recruitment and expansion of SPD-5 account for the function of centrosome-localized PLK-1. Table S1 lists the *C. elegans* strains used in this study. Table S2 presents the oligonucleotides used for dsRNA production. Table S3 lists the plasmids used in this study.

References

Alvarez-Rodrigo, I., T.L. Steinacker, S. Saurya, P.T. Conduit, J. Baumbach, Z.A. Novak, M.G. Aydogan, A. Wainman, and J.W. Raff. 2019. Evidence that a positive feedback loop drives centrosome maturation in fly embryos. *eLife*. 8:e50130. https://doi.org/10.7554/eLife.50130

Basto, R., J. Lau, T. Vinogradova, A. Gardiol, C.G. Woods, A. Khodjakov, and J.W. Raff. 2006. Flies without centrioles. *Cell*. 125:1375–1386. https://doi.org/10.1016/j.cell.2006.05.025

Baumgart, J., M. Kirchner, S. Redemann, A. Bond, J. Woodruff, J.M. Verbavatz, F. Jülicher, T. Müller-Reichert, A.A. Hyman, and J. Brugués. 2019. Soluble tubulin is significantly enriched at mitotic centrosomes. *J. Cell Biol.* 218:3977–3985. https://doi.org/10.1083/jcb.201902069

Bazzi, H., and K.V. Anderson. 2014. Acentriolar mitosis activates a p53-dependent apoptosis pathway in the mouse embryo. *Proc. Natl. Acad. Sci. USA*. 111:E1491–E1500. https://doi.org/10.1073/pnas.1400568111

Boxem, M., Z. Maliga, N. Klitgord, N. Li, I. Lemmens, M. Mana, L. de Lichtervelde, J.D. Mul, D. van de Peut, M. Devos, et al. 2008. A protein domain-based interactome network for C. elegans early embryogenesis. *Cell*. 134:534–545. https://doi.org/10.1016/j.cell.2008.07.009

Cabral, G., T. Laos, J. Dumont, and A. Dammermann. 2019. Differential Requirements for Centrioles in Mitotic Centrosome Growth and Maintenance. *Dev. Cell*. 50:355–366.e6.

Choi, Y.K., P. Liu, S.K. Sze, C. Dai, and R.Z. Qi. 2010. CDK5RAP2 stimulates microtubule nucleation by the gamma-tubulin ring complex. *J. Cell Biol.* 191:1089–1095. https://doi.org/10.1083/jcb.201007030

Citron, Y.R., C.J. Fagerstrom, B. Keszthelyi, B. Huang, N.M. Rusan, M.J.S. Kelly, and D.A. Agard. 2018. The centrosomin CM2 domain is a multi-functional binding domain with distinct cell cycle roles. *PLoS One*. 13: e0190530. https://doi.org/10.1371/journal.pone.0190530

Conduit, P.T., and J.W. Raff. 2015. Different Drosophila cell types exhibit differences in mitotic centrosome assembly dynamics. *Curr. Biol.* 25: R650–R651. https://doi.org/10.1016/j.cub.2015.05.061

Conduit, P.T., Z. Feng, J.H. Richens, J. Baumbach, A. Wainman, S.D. Bakshi, J. Dobbelaere, S. Johnson, S.M. Lea, and J.W. Raff. 2014. The centrosome-specific phosphorylation of Cnn by Polo/Plk1 drives Cnn scaffold assembly and centrosome maturation. *Dev. Cell*. 28:659–669. https://doi.org/10.1016/j.devcel.2014.02.013

Consolati, T., J. Locke, J. Roostalu, Z.A. Chen, J. Gannon, J. Asthana, W.M. Lim, F. Martino, M.A. Cvetkovic, J. Rappsilber, et al. 2020. Microtubule Nucleation Properties of Single Human γTuRCs Explained by Their Cryo-EM Structure. *Dev. Cell*. 53:603–617.e8.

Dammermann, A., T. Müller-Reichert, L. Pelletier, B. Habermann, A. Desai, and K. Oegema. 2004. Centriole assembly requires both centriolar and pericentriolar material proteins. *Dev. Cell*. 7:815–829. https://doi.org/10.1016/j.devcel.2004.10.015

Decker, M., S. Jaensch, A. Pozniakovsky, A. Zinke, K.F. O'Connell, W. Zachariae, E. Myers, and A.A. Hyman. 2011. Limiting amounts of

centrosome material set centrosome size in C. elegans embryos. *Curr. Biol.* 21:1259–1267. https://doi.org/10.1016/j.cub.2011.06.002

Dobbelaere, J., F. Josué, S. Suijkerbuijk, B. Baum, N. Tapon, and J. Raff. 2008. A genome-wide RNAi screen to dissect centriole duplication and centrosome maturation in Drosophila. *PLoS Biol.* 6:e224. https://doi.org/10.1371/journal.pbio.0060224

Enos, S.J., M. Dressler, B.F. Gomes, A.A. Hyman, and J.B. Woodruff. 2018. Phosphatase PP2A and microtubule-mediated pulling forces disassemble centrosomes during mitotic exit. *Biol. Open.* 7:bio029777. https://doi.org/10.1242/bio.029777

Feng, Z., A. Caballe, A. Wainman, S. Johnson, A.F.M. Haensele, M.A. Cottee, P.T. Conduit, S.M. Lea, and J.W. Raff. 2017. Structural Basis for Mitotic Centrosome Assembly in Flies. *Cell.* 169:1078–1089.e13.

Fong, K.W., Y.K. Choi, J.B. Rattner, and R.Z. Qi. 2008. CDK5RAP2 is a pericentriolar protein that functions in centrosomal attachment of the gamma-tubulin ring complex. *Mol. Biol. Cell.* 19:115–125. https://doi.org/10.1091/mbc.e07-04-0371

Frøkjær-Jensen, C., M.W. Davis, C.E. Hopkins, B.J. Newman, J.M. Thummel, S.P. Olesen, M. Grunnet, and E.M. Jorgensen. 2008. Single-copy insertion of transgenes in Caenorhabditis elegans. *Nat. Genet.* 40:1375–1383. https://doi.org/10.1038/ng.248

Gómez-Cavazos, J.S., K.Y. Lee, P. Lara-González, Y. Li, A. Desai, A.K. Shiau, and K. Oegema. 2020. A Non-canonical BRCT-Phosphopeptide Recognition Mechanism Underlies RhoA Activation in Cytokinesis. *Curr. Biol.* 30:3101–3115.e11. https://doi.org/10.1016/j.cub.2020.05.090

Hanafusa, H., S. Kedashiro, M. Tezuka, M. Funatsu, S. Usami, F. Toyoshima, and K. Matsumoto. 2015. PLK1-dependent activation of LRRK1 regulates spindle orientation by phosphorylating CDK5RAP2. *Nat. Cell Biol.* 17:1024–1035. https://doi.org/10.1038/ncb3204

Hannak, E., M. Kirkham, A.A. Hyman, and K. Oegema. 2001. Aurora-A kinase is required for centrosome maturation in Caenorhabditis elegans. *J. Cell Biol.* 155:1109–1116. https://doi.org/10.1083/jcb.200108051

Haren, L., T. Stearns, and J. Lüders. 2009. Plk1-dependent recruitment of gamma-tubulin complexes to mitotic centrosomes involves multiple PCM components. *PLoS One.* 4:e5976. https://doi.org/10.1371/journal.pone.0005976

Harlow, E., and D. Lane. 1988. Antibodies: A Laboratory Manual. Cold Spring Harbor Press, Cold Spring Harbor, NY.

Hattersley, N., P. Lara-Gonzalez, D. Cheerambathur, J.S. Gomez-Cavazos, T. Kim, B. Prevo, R. Khaliullin, K.Y. Lee, M. Ohta, R. Green, et al. 2018. Employing the one-cell C. elegans embryo to study cell division processes. *Methods Cell Biol.* 144:185–231. https://doi.org/10.1016/bs.mcb.2018.03.008

Huang, T.L., H.J. Wang, Y.C. Chang, S.W. Wang, and K.C. Hsia. 2020. Promiscuous Binding of Microprotein Mozart1 to γ-Tubulin Complex Mediates Specific Subcellular Targeting to Control Microtubule Array Formation. *Cell Rep.* 31:107836. https://doi.org/10.1016/j.celrep.2020.107836

Joukov, V., J.C. Walter, and A. De Nicolo. 2014. The Cep192-organized aurora A-Plk1 cascade is essential for centrosome cycle and bipolar spindle assembly. *Mol. Cell.* 55:578–591. https://doi.org/10.1016/j.molcel.2014.06.016

Kellogg, D.R., M. Moritz, and B.M. Alberts. 1994. The centrosome and cellular organization. *Annu. Rev. Biochem.* 63:639–674. https://doi.org/10.1146/annurev.bi.63.070194.003231

Kemp, C.A., K.R. Kopish, P. Zipperlen, J. Ahringer, and K.F. O'Connell. 2004. Centrosome maturation and duplication in C. elegans require the coiled-coil protein SPD-2. *Dev. Cell.* 6:511–523. https://doi.org/10.1016/S1534-5807(04)00066-8

Khodjakov, A., and C.L. Rieder. 2001. Centrosomes enhance the fidelity of cytokinesis in vertebrates and are required for cell cycle progression. *J. Cell Biol.* 153:237–242. https://doi.org/10.1083/jcb.153.1.237

Kollman, J.M., J.K. Polka, A. Zelter, T.N. Davis, and D.A. Agard. 2010. Microtubule nucleating gamma-TuSC assembles structures with 13-fold microtubule-like symmetry. *Nature.* 466:879–882. https://doi.org/10.1038/nature09207

Kollman, J.M., A. Merdes, L. Mourey, and D.A. Agard. 2011. Microtubule nucleation by γ-tubulin complexes. *Nat. Rev. Mol. Cell Biol.* 12:709–721. https://doi.org/10.1038/nrm3209

Lane, H.A., and E.A. Nigg. 1996. Antibody microinjection reveals an essential role for human polo-like kinase 1 (Plk1) in the functional maturation of mitotic centrosomes. *J. Cell Biol.* 135:1701–1713. https://doi.org/10.1083/jcb.135.6.1701

Laos, T., G. Cabral, and A. Dammermann. 2015. Isotropic incorporation of SPD-5 underlies centrosome assembly in C. elegans. *Curr. Biol.* 25:R648–R649. https://doi.org/10.1016/j.cub.2015.05.060

Lee, K., and K. Rhee. 2011. PLK1 phosphorylation of pericentrin initiates centrosome maturation at the onset of mitosis. *J. Cell Biol.* 195:1093–1101. https://doi.org/10.1083/jcb.201106093

Liu, P., E. Zupa, A. Neuner, A. Böhler, J. Loerke, D. Flemming, T. Ruppert, T. Rudack, C. Peter, C. Spahn, et al. 2020. Insights into the assembly and activation of the microtubule nucleator γ-TuRC. *Nature.* 578:467–471. https://doi.org/10.1038/s41586-019-1896-6

Magescas, J., J.C. Zonka, and J.L. Feldman. 2019. A two-step mechanism for the inactivation of microtubule organizing center function at the centrosome. *eLife.* 8:e47867. https://doi.org/10.7554/eLife.47867

Meitinger, F., J.V. Anzola, M. Kaulich, A. Richardson, J.D. Stender, C. Benner, C.K. Glass, S.F. Dowdy, A. Desai, A.K. Shiau, et al. 2016. 53BP1 and USP28 mediate p53 activation and G1 arrest after centrosome loss or extended mitotic duration. *J. Cell Biol.* 214:155–166. https://doi.org/10.1083/jcb.201604081

Meng, L., J.E. Park, T.S. Kim, E.H. Lee, S.Y. Park, M. Zhou, J.K. Bang, and K.S. Lee. 2015. Bimodal Interaction of Mammalian Polo-Like Kinase 1 and a Centrosomal Scaffold, Cep192, in the Regulation of Bipolar Spindle Formation. *Mol. Cell. Biol.* 35:2626–2640. https://doi.org/10.1128/MCB.00068-15

Mennella, V., D.A. Agard, B. Huang, and L. Pelletier. 2014. Amorphous no more: subdiffraction view of the pericentriolar material architecture. *Trends Cell Biol.* 24:188–197. https://doi.org/10.1016/j.tcb.2013.10.001

Mittasch, M., V.M. Tran, M.U. Rios, A.W. Fritsch, S.J. Enos, B. Ferreira Gomes, A. Bond, M. Kreysing, and J.B. Woodruff. 2020. Regulated changes in material properties underlie centrosome disassembly during mitotic exit. *J. Cell Biol.* 219:e201912036. https://doi.org/10.1083/jcb.201912036

Moritz, M., M.B. Braunfeld, J.W. Sedat, B. Alberts, and D.A. Agard. 1995. Microtubule nucleation by gamma-tubulin-containing rings in the centrosome. *Nature.* 378:638–640. https://doi.org/10.1038/378638a0

Moritz, M., Y. Zheng, B.M. Alberts, and K. Oegema. 1998. Recruitment of the gamma-tubulin ring complex to Drosophila salt-stripped centrosome scaffolds. *J. Cell Biol.* 142:775–786. https://doi.org/10.1083/jcb.142.3.775

Oegema, K., C. Wiese, O.C. Martin, R.A. Milligan, A. Iwamatsu, T.J. Mitchison, and Y. Zheng. 1999. Characterization of two related Drosophila gamma-tubulin complexes that differ in their ability to nucleate microtubules. *J. Cell Biol.* 144:721–733. https://doi.org/10.1083/jcb.144.4.721

Palazzo, R.E., J.M. Vogel, B.J. Schnackenberg, D.R. Hull, and X. Wu. 2000. Centrosome maturation. *Curr. Top. Dev. Biol.* 49:449–470. https://doi.org/10.1016/S0070-2153(99)49021-0

Pelletier, L., N. Ozlü, E. Hannak, C. Cowan, B. Habermann, M. Ruer, T. Müller-Reichert, and A.A. Hyman. 2004. The Caenorhabditis elegans centrosomal protein SPD-2 is required for both pericentriolar material recruitment and centriole duplication. *Curr. Biol.* 14:863–873. https://doi.org/10.1016/j.cub.2004.04.012

Pintard, L., and B. Bowerman. 2019. Mitotic Cell Division in *Caenorhabditis elegans*. *Genetics.* 211:35–73. https://doi.org/10.1534/genetics.118.301367

Ponting, C.P. 2006. A novel domain suggests a ciliary function for ASPM, a brain size determining gene. *Bioinformatics.* 22:1031–1035. https://doi.org/10.1093/bioinformatics/btl022

Sallee, M.D., J.C. Zonka, T.D. Skokan, B.C. Raftrey, and J.L. Feldman. 2018. Tissue-specific degradation of essential centrosome components reveals distinct microtubule populations at microtubule organizing centers. *PLoS Biol.* 16:e2005189. https://doi.org/10.1371/journal.pbio.2005189

Samejima, I., V.J. Miller, L.M. Groocock, and K.E. Sawin. 2008. Two distinct regions of Mto1 are required for normal microtubule nucleation and efficient association with the γ-tubulin complex in vivo. *J. Cell Sci.* 121:3971–3980. https://doi.org/10.1242/jcs.038414

Schnackenberg, B.J., A. Khodjakov, C.L. Rieder, and R.E. Palazzo. 1998. The disassembly and reassembly of functional centrosomes in vitro. *Proc. Natl. Acad. Sci. USA.* 95:9295–9300. https://doi.org/10.1073/pnas.95.16.9295

Shimanovskaya, E., V. Viscardi, J. Lesigang, M.M. Lettman, R. Qiao, D.I. Svergun, A. Round, K. Oegema, and G. Dong. 2014. Structure of the C. elegans ZYG-1 cryptic polo box suggests a conserved mechanism for centriolar docking of Plk4 kinases. *Structure.* 22:1090–1104. https://doi.org/10.1016/j.str.2014.05.009

Sir, J.H., M. Pütz, O. Daly, C.G. Morrison, M. Dunning, J.V. Kilmartin, and F. Gergely. 2013. Loss of centrioles causes chromosomal instability in vertebrate somatic cells. *J. Cell Biol.* 203:747–756. https://doi.org/10.1083/jcb.201309038

Sugioka, K., D.R. Hamill, J.B. Lowry, M.E. McNeely, M. Enrick, A.C. Richter, L.E. Kiebler, J.R. Priess, and B. Bowerman. 2017. Centriolar SAS-7 acts

upstream of SPD-2 to regulate centriole assembly and pericentriolar material formation. *eLife*. 6:e20353. https://doi.org/10.7554/eLife.20353

Wieczorek, M., T.L. Huang, L. Urnavicius, K.C. Hsia, and T.M. Kapoor. 2020a. MZT Proteins Form Multi-Faceted Structural Modules in the γ-Tubulin Ring Complex. *Cell Rep*. 31:107791. https://doi.org/10.1016/j.celrep.2020.107791

Wieczorek, M., L. Urnavicius, S.C. Ti, K.R. Molloy, B.T. Chait, and T.M. Kapoor. 2020b. Asymmetric Molecular Architecture of the Human γ-Tubulin Ring Complex. *Cell*. 180:165–175.e16.

Wong, Y.L., J.V. Anzola, R.L. Davis, M. Yoon, A. Motamedi, A. Kroll, C.P. Seo, J.E. Hsia, S.K. Kim, J.W. Mitchell, et al. 2015. Reversible centriole depletion with an inhibitor of Polo-like kinase 4. *Science*. 348:1155–1160. https://doi.org/10.1126/science.aaa5111

Woodruff, J.B., O. Wueseke, and A.A. Hyman. 2014. Pericentriolar material structure and dynamics. *Philos. Trans. R. Soc. Lond. B Biol. Sci.* 369: 20130459. https://doi.org/10.1098/rstb.2013.0459

Woodruff, J.B., O. Wueseke, V. Viscardi, J. Mahamid, S.D. Ochoa, J. Bunkenborg, P.O. Widlund, A. Pozniakovsky, E. Zanin, S. Bahmanyar, et al. 2015. Regulated assembly of a supramolecular centrosome scaffold in vitro. *Science*. 348:808–812. https://doi.org/10.1126/science.aaa3923

Woodruff, J.B., B. Ferreira Gomes, P.O. Widlund, J. Mahamid, A. Honigmann, and A.A. Hyman. 2017. The Centrosome Is a Selective Condensate that Nucleates Microtubules by Concentrating Tubulin. *Cell*. 169: 1066–1077.e10.

Xue, Y., F. Zhou, M. Zhu, K. Ahmed, G. Chen, and Y. Xuebiao. 2005. GPS: a comprehensive www server for phosphorylation sites prediction. *Nucleic Acids Res*. 33:W184–W187. https://doi.org/10.1093/nar/gki393

Zhang, J., and T.L. Megraw. 2007. Proper recruitment of gamma-tubulin and D-TACC/Msps to embryonic Drosophila centrosomes requires Centrosomin Motif 1. *Mol. Biol. Cell*. 18:4037–4049. https://doi.org/10.1091/mbc.e07-05-0474
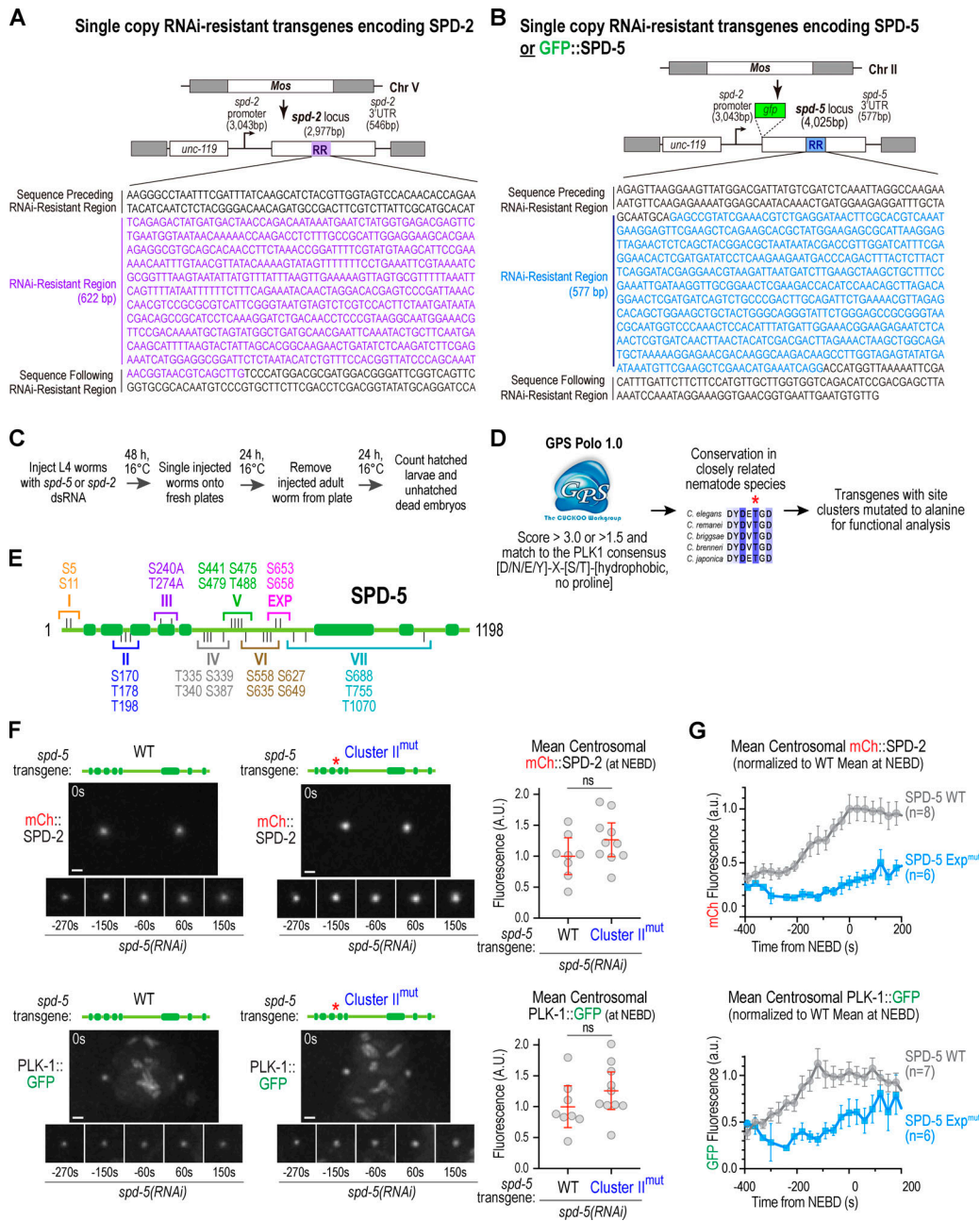
Supplemental material

Figure S1. **Transgene replacement systems for SPD-2 and SPD-5, method for identifying putative PLK-1 sites in SPD-5, and analysis of PLK-1 and SPD-2 centrosomal localization in Cluster II[mut] and Exp[mut] SPD-5. (A and B)** Single-copy RNAi-resistant transgene insertion systems used to express SPD-2 (A) and SPD-5 (B) variants. Regions marked "RR" were altered in nucleotide but not in protein coding sequence to make the transgene-encoded products resistant to dsRNAs targeting the equivalent region of the endogenous genes. Due to the repetitive architecture of the *spd-5* promoter region, the *spd-2* promoter was used to control expression of the *spd-2* and *spd-5* transgenes. **(C)** Protocol employed to assess embryonic lethality. L4 worms were injected with dsRNA targeting *spd-5* or *spd-2*, and embryos laid 48–72 h (at 16°C) after injection were scored for lethality. **(D)** Outline of procedure used to identify putative PLK-1 target sites in SPD-5. Red asterisk marks the phosphorylation site. **(E)** Schematic depicting identified sites and regional clusters employed for mutagenesis. Seven transgenes harboring mutant clusters I–VII were used to generate single-copy integration strains that were used for the embryonic lethality analysis shown in Fig. 2 A. **(F)** Images of in situ–tagged mCherry::SPD-2 (top) and PLK-1::GFP (bottom) in embryos expressing WT or Cluster II[mut] SPD-5 after endogenous SPD-5 depletion. Red asterisks mark the Cluster II mutation site in SPD-5. Times in the top left of large panels and below smaller panels are in seconds relative to NEBD. Scale bars, 2 μm. Graphs on right show quantification of centrosomal mCherry (mCh)::SPD-2 or PLK::GFP signal at NEBD. Error bars are mean with 95% confidence intervals. P values are from two-tailed *t* tests. **(G)** Centrosomal fluorescence of mCherry::SPD-2 (top) and PLK-1::GFP (bottom) in embryos expressing WT or Exp[mut] SPD-5 after endogenous SPD-5 depletion. Values were plotted after normalizing to the mean at NEBD for WT SPD-5. Error bars are the SEM; *n* is the number of centrosomes quantified. SPD-2 is recruited to centrioles by binding to the C-terminus of SAS-7 (Sugioka et al., 2017) and is thought to associate with the PCM matrix via a direct association with SPD-5 (Boxem et al., 2008). Consistent with this, levels of centrosomal mCherry::SPD-2 and PLK-1::GFP are similar in embryos expressing WT and Exp[mut] SPD-5 before mitotic entry and expansion of the SPD-5 matrix. After mitotic entry, mCherry::SPD-2 levels at centrosomes increase as the WT SPD-5 matrix expands, and this increase fails to occur in Exp[mut] SPD-5 embryos. unc, uncoordinated; NEBD, nuclear envelope breakdown.
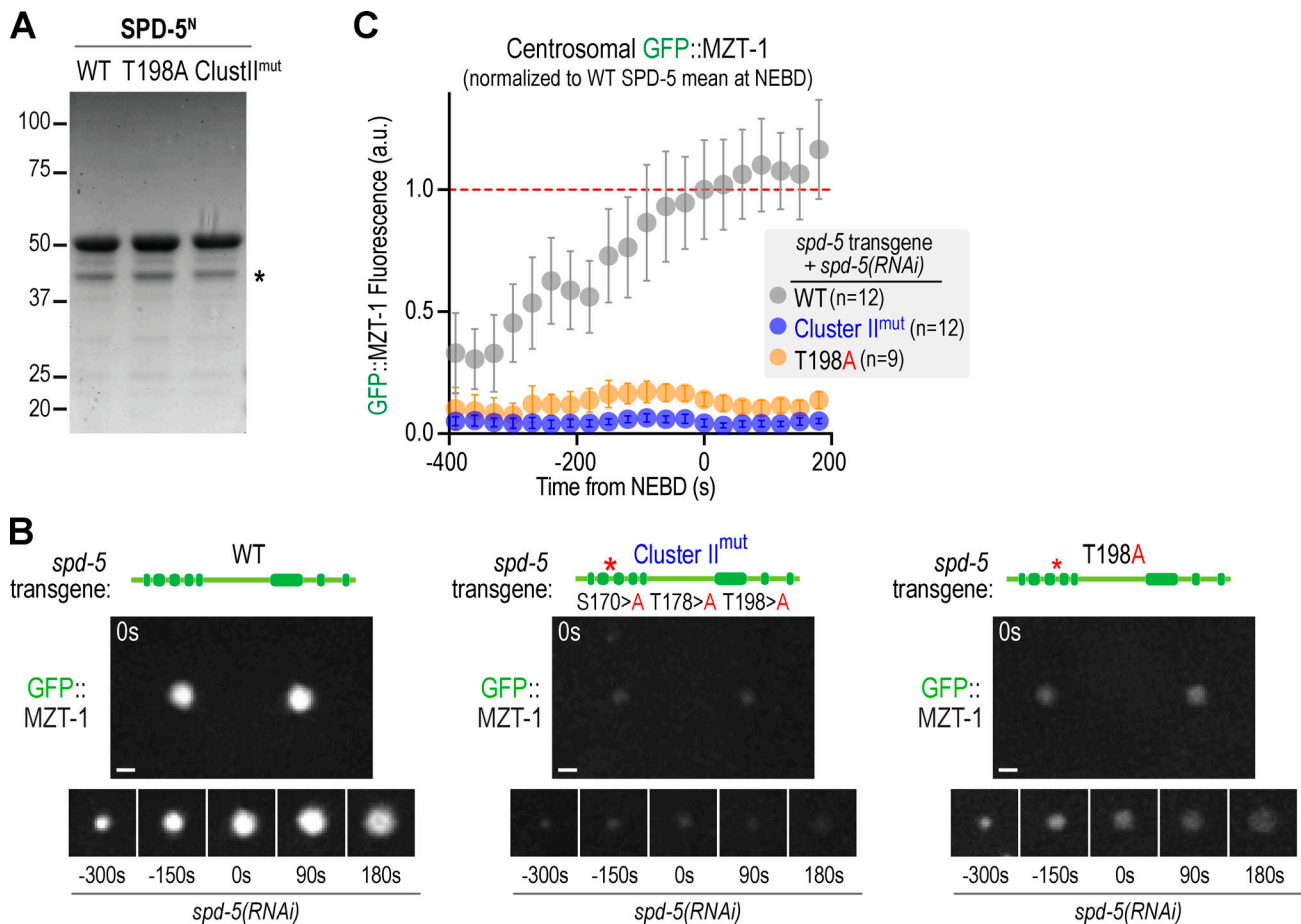
Figure S2.   **Related to** Fig. 3: **Analysis of GFP::MZT-1 localization. (A)** Coomassie blue–stained gel showing the purified SPD-5 N-terminal fragments (aa 1–473, SPD-5^N) used in the interaction assays. Asterisk marks a SPD-5^N breakdown product. **(B)** Images of in situ–tagged GFP::MZT-1 for the indicated conditions. Red asterisks mark the mutated sites in SPD-5. Times shown in top left of large panels and below smaller panels are in seconds relative to NEBD. Scale bar, 2 µm. **(C)** Quantification of centrosomal GFP::MZT-1 signal. Values were normalized relative to the mean at NEBD in the presence of WT SPD-5. Error bars are the 95% confidence intervals. *n* refers to the number of centrosomes. Clust, Cluster; NEBD, nuclear envelope breakdown.
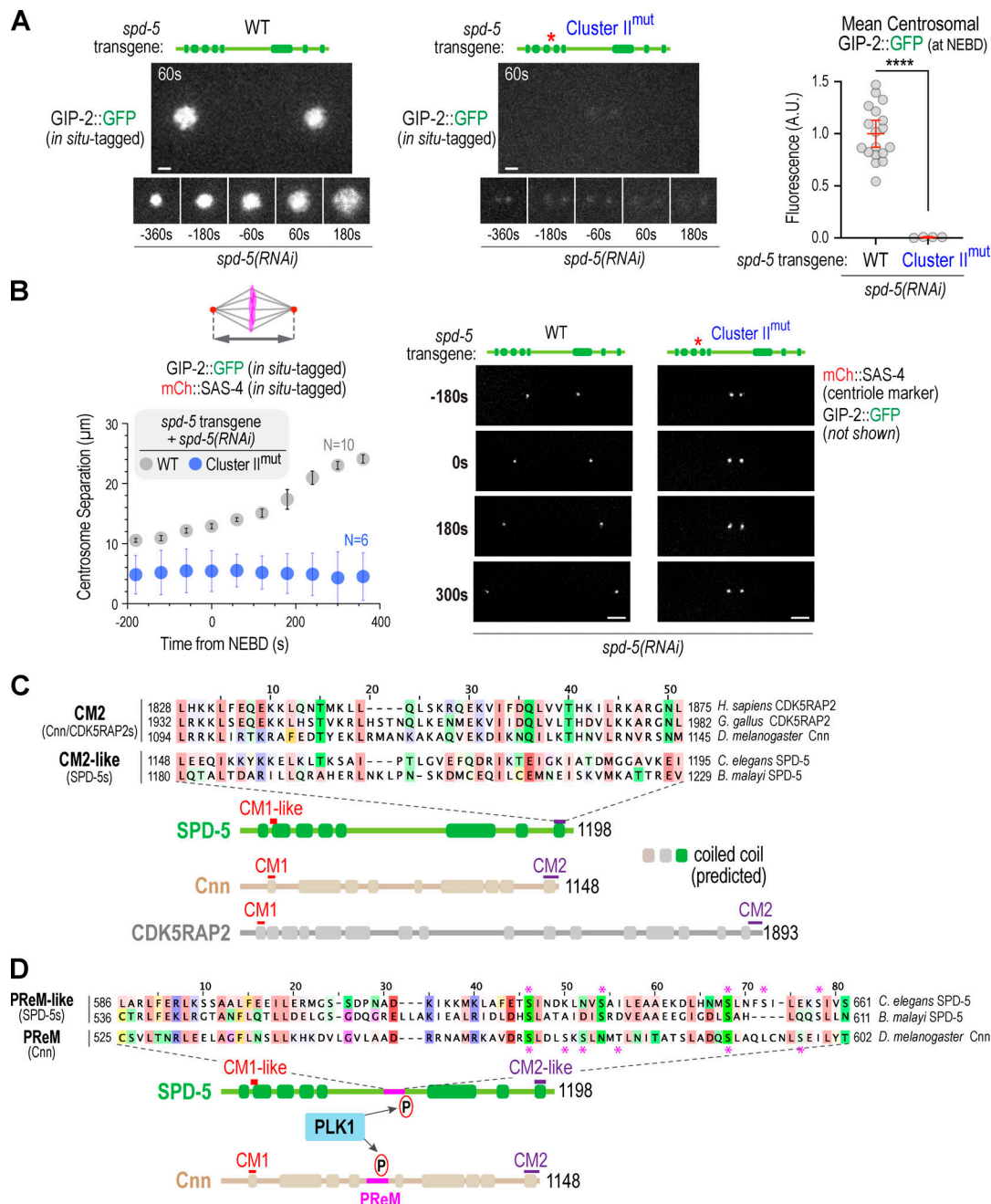
Figure S3. **Related to** Fig. 4: **In situ–tagged GIP-2::GFP exhibits a synthetic spindle assembly phenotype when combined with Cluster II^mut SPD-5. (A)** Example images of GIP-2::GFP in the presence of WT or Cluster II^mut SPD-5. Times in the top left of large panels and below smaller panels are seconds relative to NEBD. Scale bar, 2 μm. Error bars are mean with 95% confidence intervals. P values are from two-tailed t tests. Red asterisk marks the location of the Cluster II mutation in SPD-5. **(B)** Quantification of centrosome separation for the indicated conditions. Spindle length was measured using mCherry (mCh)::SAS-4 that was also expressed in the analyzed strains. Times are seconds after NEBD. Error bars are the 95% confidence intervals. N refers to number of embryos imaged. Red asterisk marks the location of the Cluster II mutation in SPD-5. Scale bar, 3 μm. **(C and D)** Nematode SPD-5s have regions with homology to the domains of *Drosophila* Cnn that mediate its PLK-1–regulated self-assembly. Expansion of the Cnn-based PCM matrix occurs through a phospho-regulated self-interaction in which a conserved CM2 motif at the Cnn C-terminus interacts with an internal region of Cnn (called the phospho-regulated multimerization or "PReM" domain) composed of a leucine zipper followed by a control region that enables assembly when phosphorylated by PLK-1 (Citron et al., 2018; Conduit et al., 2014; Feng et al., 2017). **(C)** Sequence alignment suggesting the presence of a CM2-like domain at the SPD-5 C-terminus. **(D)** Sequence alignment showing the region of SPD-5 containing the PLK-1 sites previously shown to control SPD-5 self-assembly (S653 and S658; Woodruff et al., 2015). Pink asterisks mark candidate PLK-1 sites predicted by GPS (Group-based Prediction System) Polo (Xue et al., 2005) with a score >2.165. In preliminary work (not shown), we found that mutant VI (Fig. 2A and Fig. S1 E) also leads to an Exp^mut-like phenotype, suggesting that some of the other PLK-1 sites in this region may also be essential for PCM assembly. The locations of the PLK1 site clusters that control the assembly of *C. elegans* SPD-5 and *Drosophila* Cnn are indicated on the schematics with red-circled Ps. Like the PLK-1 sites in the PReM region required for Cnn assembly (Conduit et al., 2014), the functionally important PLK1 sites in the *C. elegans* protein follow a short leucine-rich region. NEBD, nuclear envelope breakdown; PReM, phospho-regulated multimerization. *B. malayi, Brugia malayi; G. gallus, Gallus gallus; H. sapiens, Homo sapiens.*

Video 1. **Centrosomal PLK-1 is required for PCM expansion during mitotic entry.** Spinning disk confocal optics were used to image one-cell–stage *C. elegans* embryos expressing in situ–tagged PLK-1::GFP (green) and mCherry::SPD-5 (magenta) in the presence of transgene-encoded WT or PD^{mut} SPD-2; endogenous SPD-2 was depleted. Times shown in bottom left are seconds after nuclear envelope breakdown (NEBD). 11 × 1–μm z-stacks were acquired every 60 s, and maximal intensity projections were generated for each time frame. Playback rate is two frames per second. Embryos were filmed at 20°C. Scale bar, 10 μm. Related to Fig. 1 B.

Video 2. **Putative PLK-1 target site Cluster II^{mut} SPD-5 did not block PCM expansion.** Spinning disk confocal optics were used to image one-cell–stage *C. elegans* embryos expressing transgene-encoded GFP fusion with WT, Cluster II^{mut}, or Exp^{mut} SPD-5; endogenous SPD-5 was depleted. Times shown in bottom left are seconds after nuclear envelope breakdown (NEBD). 6 × 2–μm z-stacks were acquired every 30 s, and maximal intensity projections were generated for each time frame. Playback rate is two frames per second. Embryos were filmed at 20°C. Scale bar, 10 μm. Related to Fig. 1 C; and Fig. 2, B–D and I.

Video 3. **PLK-1 target site Cluster II in SPD-5 is required to dock γ-tubulin complexes onto the PCM matrix.** Spinning disk confocal optics were used to image one-cell–stage *C. elegans* embryos expressing transgene-encoded γ-tubulin::mCherry in the presence of transgene-encoded untagged WT, Cluster II^{mut}, Exp^{mut}, or T198A SPD-5; endogenous SPD-5 was depleted. Times shown in bottom left are seconds after nuclear envelope breakdown (NEBD). 13 × 1–μm z-stacks were acquired every 30 s, and maximal intensity projections were generated for each time frame. Playback rate is two frames per second. Embryos were filmed at 20°C. Scale bar, 10 μm. Related to Fig. 2, E–G; and Fig. 3 H.

Video 4. **PLK-1–controlled γ-tubulin recruitment and expansion of SPD-5 account for the function of centrosome-localized PLK-1.** Spinning disk confocal optics were used to image one-cell–stage *C. elegans* embryos expressing transgene-encoded GFP::β-tubulin (green) and mCherry::histone (magenta) in the presence of transgene-encoded untagged WT or PLK-1–docking mutant (PD^{mut}) SPD-2, or WT, Cluster II^{mut}, Exp^{mut}, or Cluster II^{mut} and Exp^{mut} SPD-5; endogenous SPD-2 or SPD-5 was depleted. Times shown in bottom left are seconds after nuclear envelope breakdown (NEBD). 11 × 1–μm z-stacks were acquired every 60 s for SPD-2 variants; 9 × 1–μm z-stacks were acquired every 30 s for SPD-5 variants. For microtubule imaging, the three z-planes containing the spindle poles were projected for each time point. For mCherry::histone, all z-planes were projected for each time point. Playback rate is two frames per second. Embryos were filmed at 20°C. Scale bar, 10 μm. Related to Fig. 4, A and B.

Provided online are three tables. Table S1 lists the *C. elegans* strains used in this study. Table S2 presents the oligonucleotides used for dsRNA production. Table S3 lists the plasmids used in this study.